Article

Climate Change Impact in the Ria de Aveiro Lagoon Ecosystem: A Case Study

José Fortes Lopes [1,]* , **Carina Lurdes Lopes [1,2]** and **João Miguel Dias [1]**

[1] CESAM, Universidade de Aveiro, 3810-193 Aveiro, Portugal; carinalopes@ua.pt (C.L.L.);
    joao.dias@ua.pt (J.M.D.)
[2] MARE, Universidade de Lisboa, 1749-016 Lisboa, Portugal
* Correspondence: jflopes@ua.pt; Tel.: +351-234-370-821

check for updates

Abstract: Climate change and global sea-level rise are major issues of the 21st century. The main goal of this study is to assess the physical and biogeochemical status of the Ria de Aveiro lagoon (Portugal) under future climate scenarios, using a coupled physical/ eutrophication model. The impact on the lagoon ecosystem status of the mean sea level rise (MSLR), the amplitude rise of the M2 tidal constituent (M2R), the changes in the river discharge, and the rising of the air temperature was investigated. Under MSLR and M2R, the results point to an overall salinity increase and water temperature decrease, revealing ocean water dominance. The main lagoon areas presented salinity values close to those of the ocean waters (~34 PSU), while a high range of salinity was presented for the river and the far end areas (20–34 PSU). The water temperature showed a decrease of approximately 0.5–1.5 °C. The responses of the biogeochemical variables reflect the increase of the oceanic inflow (transparent and nutrient-poor water) or the reduction of the river flows (nutrient-rich waters). The results evidenced, under the scenarios, an overall decreasing of the inorganic nitrogen concentration and the carbon phytoplankton concentrations. A warm climate, although increasing the water temperature, does not seem to affect the lagoon's main status, at least in the frame of the model used in the study.

Keywords: climate change; sea level rise; salinity; water temperature; phytoplankton; inorganic nitrogen

1. Introduction

Climate change due to global warming, resulting from past and ongoing emissions of anthropogenic carbon, is one of the major issues of the 21st century. Because air temperature increases more quickly over land than over oceans, coastal water temperature is also likely to increase more rapidly [1]. Nevertheless, the temperature will rise differently worldwide due to both natural variability and regional influence, with higher latitudes expected to be more affected [2,3]. The global mean temperature has increased by 0.85 °C (likely between 0.65 °C and 1.06 °C) between 1880 and 2012 [4] and is expected to increase by an additional 0.3–4.8 °C by 2100 [5]. The sea surface water temperature increased between 1971 and 2010 at an average rate of 0.11 °C/decade [6] and is expected to increase by an additional 0.6–2.0 °C by 2100 [5].

Several natural and anthropogenic processes related to climate changes may affect coastal ecosystems, like the Ria de Aveiro lagoon. Kumbier et al. [7] investigated the hydrodynamic impacts of sea level rise (SLR) on wave-dominated Australian estuaries with differing geomorphology and found that SLR will affect the hydrodynamics and flooding characteristics of those systems. Their geomorphology together with drivers such as spring tides, storm surges, and river inflows constitute the major forcing. They point out that estuarine response to SLR varies between different types of estuaries and that floodplain elevation seems to be the fundamental factor for identifying the

most vulnerable systems and estimating how inundation extents and depths may change in response to SLR. In particular, it seems that mature and immature estuaries [7] will have different responses to SLR. While the former may experience a considerable increase in inundation depths, the latter may be subject to increases in relative inundation extent and substantial changes in hydrodynamics such as tidal range and current velocity. They concluded, therefore, that the response of estuarine systems to SLR is crucially dependent on their geomorphology. Huber and Gulledge [8] pointed out that the combination of observed trends, theoretical understanding of climate system, and numerical modelling demonstrate that global warming is increasing the risk of extreme weather and climate events (ECEs), whereas Ummenhofer and Meehl [9] reviewed ECEs with ecology relevant for terrestrial, atmospheric and oceanic ecosystems, pointing to the importance of a continued development of models that simulate biogeochemical cycles and interactions with the biosphere, making it possible to develop a mechanistic understanding of how ECEs affect biological processes, ecosystem functioning, and adaptation capabilities. ECEs, such as heatwaves or prolonged episodes of dryness, heavy rainfall and major river floods, storm surge, and waves, are likely to affect coastal systems, namely their morphodynamics, as well as the physics and the biogeochemistry of the water column, on both daily and seasonal time scales [10]. Furthermore, the anthropogenic pressure and land-use changes are, as well, very likely to continue impacting those systems, increasing their exposition and vulnerabilities to natural events.

Global Sea Level Rise, SLR, is an important consequence of global warming, glaciers melting, and expansion of the ocean waters [11,12]. The ice loss from glaciers between 1993 and 2009, measured in terms of sea-level equivalent, is estimated to be about 13 mm. The rate of ice loss from the Greenland ice sheet is estimated to be about 0.59 (0.43 to 0.76) mm yr^{-1}, over the period 2002–2011 [13]. Despite the uncertainty in the sea level rise projections [14,15], estimations supported on tide gauge records and satellite data indicate that the mean sea level, MSL, has risen by 0.19 (0.17 to 0.21) m over the period 1901–2010 [10], and projections based on climate models evidence an additional rise between 0.26 and 0.82 m, by 2100 [5]. Concerning the Portuguese coast, Antunes and Taborda [16], analysing the Cascais tidal gauge data, found a rate of increase of the mean sea level rise, MSLR, of 2.1 ± 0.1 mm/yr and projected a cumulated rise of 0.47 m with a 95% confidence interval between 0.19 and 0.75 m at the year 2100 relative to the 1990 mean sea level [17].

Recent studies highlighted the effect of *SLR* on the components of the tide. Pelling et al. [18,19], Pickering et al. [20], and Idier et al [21] reported a non-linear response of tides to the SLR for the European Shelf and anticipated an increase or a decrease of the M_2 (principal semidiurnal lunar tidal constituent) amplitude for different North Sea areas, pointing out that the signs and that the magnitudes of the changes may display local discrepancies.

SLR is expected to impact coastal water systems, like barrier lagoons, inducing their migration landward [22] and increasing the vulnerability of the shallow areas to inundation [23]. It will also contribute to the increase of the rate of exchange with the ocean [22], and of the lagoons' and estuaries' flushing rates [24], which may affect the water column properties, namely the salinity, the water temperature, the nutrient budget, the turbidity, and the light penetration [25]. Changes in the radiative and thermal fluxes between the atmosphere and the water will affect the water temperature of the shallow water [26–29], influencing, in turn, the dissolved oxygen content of the water column, whose concentration decreases with the temperature increase. While lagoons with high flushing rates or low residence time may mitigate these effects, through the tidal transport of water and the turbulent mixing [30], shallow areas of slow-moving water and high residence times might be the most affected. Furthermore, the increase of water temperature, salinity and hypoxia can affect the species composition (the biodiversity), namely the benthic community ecosystems [31,32], by changing the species diversity and shifting the composition for more temperature, salty or hypoxia-tolerant species [33–35]. Warmer water temperature is reported to contribute to the declining of the phytoplankton abundance due to increased grazing by zooplankton [33], as well as the declining of the seagrass abundance [36]. Pearl and Valerie [37] investigated the relationship between the

global expansion of harmful cyanobacteria and climate and anthropogenic changes in coastal water systems characterized by freshwater and marine influences. They found that, as climate changes affect thermal and hydrologic regimes of those systems, cyanobacterial blooms may become a persistent challenge to their water quality as well as to the fisheries management. On the other hand, it seems that mature and immature estuaries will have different responses to SLR. While the former may experience a considerable increase in inundation depths, the latter may be subject to increases in relative inundation extent and substantial changes in hydrodynamics such as tidal range and current velocity. They concluded, therefore, that the response of estuarine systems to SLR is crucially dependent on their geomorphology.

Attending these concerns, this work aims to understand how the physical (salinity and water temperature) and the biogeochemical patterns of the Ria de Aveiro lagoon will be affected by the future climate. Based on the climate change scenarios for the Portuguese and the Aveiro coastal area, their impact on the physical and biogeochemical status of the lagoon ecosystem was investigated. In particular, the impact of SLR and the amplitude of tide changes at the lagoon mouth, on the salinity, the water temperature, and the biogeochemical state variables was considered.

The study was performed with the help of a physical/eutrophication model (Mike3, 2009) [38,39], which simulates the hydrodynamics, the salinity, the temperature and the main biogeochemical variables associated with the lower trophic level of the water column, namely, phytoplankton, nutrients (N, P), detritus and dissolved oxygen. It includes, as well, rooted vegetation and zooplankton.

Previous studies concerning the lagoon hydrodynamic status under future climate scenarios were performed by Lopes and Dias [40,41], Lopes et al. [42,43], and Vargas et al. [44]. Lopes and Dias [40] studied the influence of the mean sea level rise, MSLR, on the lagoon tidal dynamics through numerical modelling. They found that MSLR will change the tidal propagation within the lagoon, projecting an increase of the amplitude of the M_2 constituent and a decrease of the phase. Lopes et al. [42,43] and Lopes and Dias [40,41] investigated the influence of MSLR on the lagoon water levels and inundation patterns and found that MSLR will increase the water levels and the extension of the flooded areas, endangering the main lagoon margins. The studies further highlight that the margins holding agricultural activities are highly vulnerable to saltwater intrusion. Vargas et al. [44] studied the influence of MSLR and river inflow changes on the Ria de Aveiro salinity patterns through numerical modelling. They found that the projected MSLR and river flow decrease will increase the salinity all over the lagoon, with saline fronts displacing further upstream.

2. The Study Area

The research was focused on the Ria de Aveiro (Figure 1) lagoon, an area widely studied and used as a natural laboratory for several inter-disciplinary research activities [40–50]. It is a lagoon located on the Northwest Atlantic coast of Portugal (40°38′ *N*, 8°45′ *W*), 45 km long and 10 km wide, covering an area ranging from 66 to 83 km^2, at low and high tide, respectively. It is a very shallow system (average depth of 1 m) characterised by four main channels (S. Jacinto, Espinheiro, Mira and Ílhavo) that are directly connected to the lagoon mouth and the ocean by a single tidal channel. The central part of the lagoon is constituted by a myriad of other small channels dominated by shallow and tidal flat areas, contributing to strong damping of the currents and an increase of the phase delay of the tidal wave.
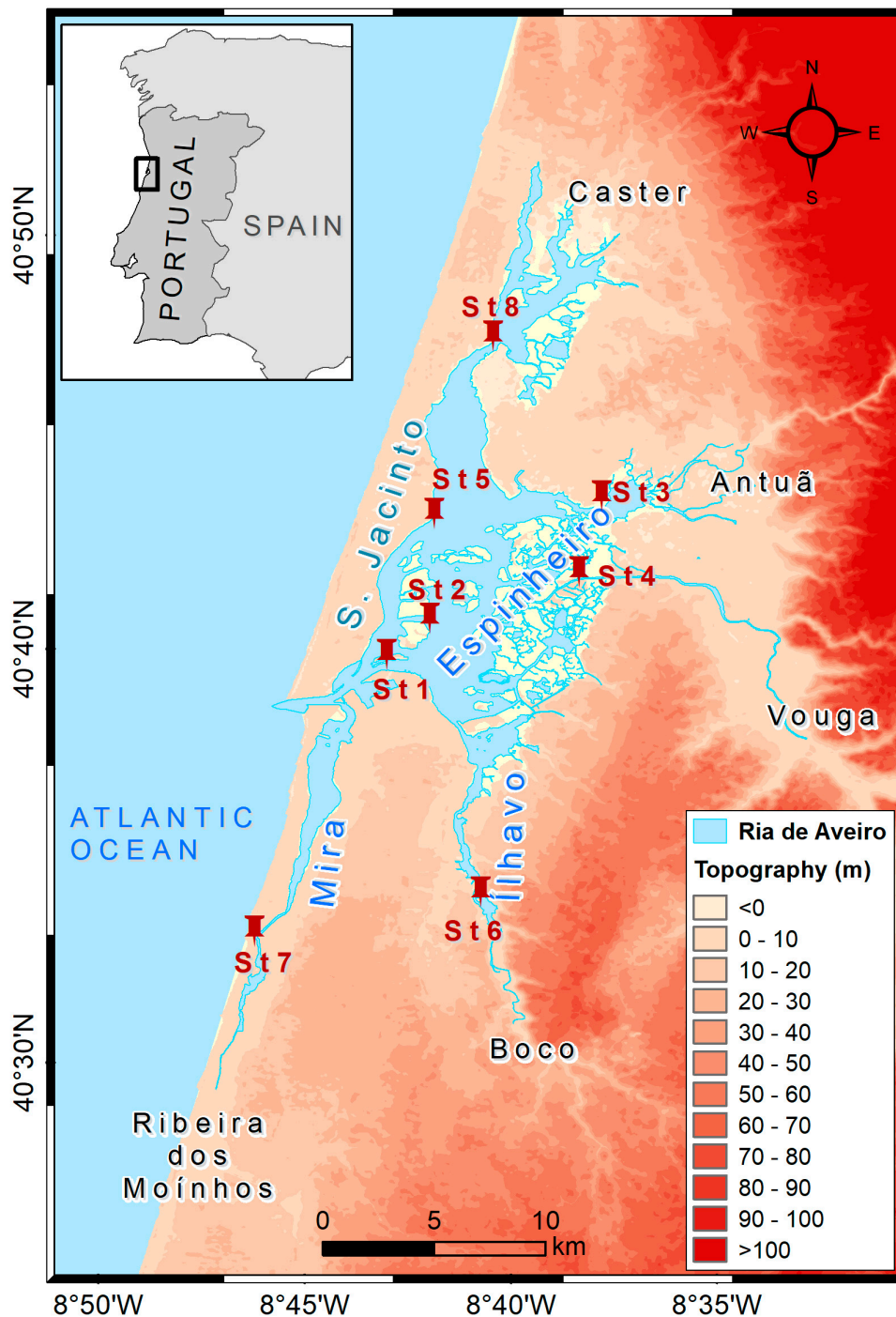
Figure 1. The study area: the Ria de Aveiro lagoon, with the location of the stations (St1 to St7).

The lagoon is a shallow water and well-mixed system, except near the lagoon mouth, where some stratifications are observed, resulting from the water confluence of the ocean saltwater and mix-water from the Espinheiro channel, which is connected to the Vouga river [44,45]. The tide is semidiurnal inducing sea level variations at the lagoon mouth between 0.45 m and 3.80 m. Dias [45], Vaz and Dias [46], Dias et al. [47–49], and Dias and Lopes [50] characterised the lagoon in two main areas: (1) the central area under the influence of the tide, characterised by strong currents, along the S. Jacinto and the Espinheiro channels, particularly close to the lagoon mouth where the intensity of the currents may reach values higher than 2 m s^{-1}, which progressively decrease toward the inner areas of the channels, (2) the far end channels, which are mainly very shallow intertidal areas, where the currents

reach low values ($\sim$ 0.1 m s^{-1}) and the residence time is about two weeks. Dias [45] showed that the lagoon is ebb dominant at the mouth and central areas and flood dominant at the far ends.

Winds and waves play a minor role in local hydrodynamics when compared to the tides. Fortunato et al. [51] found that the maximum contribution of wind stress on water levels is typically lower than 0.05 m. Vaz et al. [52] found that waves with significant height (4 m) only produce elevations of approximately 0.2 m. The lagoon has suffered several changes in the past caused by both natural and anthropogenic factors that locally reconfigure its morphology, affecting the tidal propagation and the hydrodynamics [40–43]. The amplitude of M_2 tidal constituent has increased by a rate of 2.8 mm yr^{-1} between 1976 and 2013 as a consequence of the main channels deepening [39–41]. The same study found that the sea level increased at a rate of 2.2 $\pm$ 0.1 mm yr^{-1} at the lagoon entrance.

Two main rivers, Vouga and Antuã, situated at the eastern boundary of the lagoon, are the main tributaries of freshwater. In addition to these, there are other small, less important rivers: Cáster (situated at the northern boundary), Boco (situated at the southern boundary) and Ribeira dos Moínhos (Mira), [45–47]. Vicente [53], suggested that the average flow for the Vouga and the Antuã rivers is 50 m^3 s^{-1} and 5 m^3 s^{-1}, respectively, while more recently Génio et al. [54] set the values to 80 m^3 s^{-1} and 20 m^3 s^{-1}. Concerning Ribeira dos Moínhos, Cáster, and Boco rivers, the same authors estimated daily mean discharges of about 10, 5 and 0.5 m^3 s^{-1}, respectively. The total mean river discharge during a tidal cycle was estimated by Moreira et al. [55] in 1.89×10^6 m^3, which is considerably lower than the tidal prism at the lagoon mouth, of about 65.89×10^6 and 139.79×10^6 m^3, for neap and the spring tide conditions, respectively [40–43]. In general, fluvial inputs to the lagoon occur at a small steady flow, with the discharge values close to the mean values. During the wet season (spring and autumn), the sudden increase of the river tributaries generates intense river pulses or flash floods. In particular, the Vouga river transient runoff may generate peak discharge values up to 120 m^3 s^{-1} [46].

Concerning nutrients, high values of nitrate and nitrites ($NO_3 + NO_2$) concentrations (of the order or higher than 3.5 mg L^{-1}) and phosphates (PO_4) (maximum value 0.4 mg L^{-1}) were reported for 2000 and 2001 by Almeida et al. [56], Rodrigues et al. [57], Lopes et al. [58–60] and Silva et al. [61] (most of the data was obtained in the framework of the ModelRia project [62], an integrated multidisciplinary project (2000/2001) with the purpose of better understanding the lagoon physical and biogeochemical functioning). Data cover the same stations as presented in Figure 1, but do not correspond to a continuous record, but rather a limited number of days, during high and low tide (March, June, September, and December). Indeed, since rivers are the main source of nutrients, the sampling strategy may have been designed to capture the extreme concentration values associated with intraday and seasonal variabilities of the lagoon. Nitrate and nitrites ($NO_3 + NO_2$) concentration increased from minimum values, below 0.1 mg L^{-1}, close to the lagoon mouth, to maximum values ($>$1.0 mg L^{-1}) close to the river mouths. The concentration of phosphates (PO_4) follows a similar trend, reaching a maximum value of $\sim$0.4 mg L^{-1} close to the river mouths, which points to a riverine origin of the nutrients in the lagoon [56]. Almeida et al. [56] reported that the *N/P* ratio inside the lagoon is generally high ($>$4). In 2000 and 2001 extremely high ratio values were observed ($\sim$350) at *St3* and *St4*, and high values ($>$20) elsewhere. This emphasises the importance of the *N* cycle inside the lagoon. The carbon phytoplankton concentration (*PC*), which quantifies the phytoplankton biomass in carbon, and the chlorophyll-a (*Chl-a*) ranged, respectively, within (0.1–1.0 mg L^{-1}) and (0.1–60 μg L^{-1}) [62]; the maximum values were observed during summer 2000 [56].

Extreme climatological events are becoming more frequent in the study area, alternating abnormal situations of dry or wet and warm or cold weather, leading to severe situations of high or low river runoffs and flash floods, as was the case in late summer 2000 and winter 2000/spring 2001, respectively [56–60,62]. They depict situations for which the lagoon shifted from typical conditions to ones dominated by the ocean or the river waters. In this situation, extreme values and high gradient values of the main physical and biogeochemical variables are observed. Summer 2000 represented a typical dry situation, showing high salinity values (34 PSU), whereas the wet winter 2000 and spring 2001 presented episodes of extremely low salinity values ($<$10), observed even close to the lagoon

mouth. High values of nitrate and nitrites were observed (>3.5 mg L^{-1}) at the main river's boundaries, as well as at the main lagoon stations.

3. Material and Methods

3.1. The Models

The model is very similar to the one used in previous studies [58,59]. It consists of a coupled *3D* hydrodynamic/eutrophication model, Mike3 [38,39], from the Danish Hydraulic Institut (DHI), which includes eutrophication and water quality modules, that is applied to simulate the physical and the biogeochemical status of the lagoon. The hydrodynamic model solves the three-dimensional incompressible Reynolds averaged Navier-Stokes equations, assuming the Boussinesq and hydrostatic pressure approximations, and the general transport-diffusion equations applied to the water temperature, *T*, the salinity, *S*, and a given scalar quantity C. Heat and radiative fluxes are imposed at the free surface, namely the incident solar radiation Q_S and the non-solar Q_{LW} net longwave radiation emitted by the water surface. The Q_S is assessed with the help of the Ångström-Prescott model [63], which estimates the extra-terrestrial radiation on the horizontal surface.

The eutrophication module integrates the phytoplankton and the macroalgae as well as the nutrient cycles (nitrogen, *N*, and phosphorus, *P*) [38,39]. Furthermore, it also includes rooted vegetation and a zooplankton compartment. The mass balance for the benthic vegetation includes production and losses. It includes, as well, biogeochemical processes occurring in the upper sediment surface layer: nutrients (*N* and *P*) can be exchanged between the bottom sediment layer and the water column, affecting the water column budget. The model is represented by four functional groups (phytoplankton, zooplankton, benthic vegetation and detritus), including the nutrients and oxygen budgets, and simulates the following states variables: phytoplankton, chlorophyll-a, zooplankton, organic matter (detritus), organic and inorganic nutrients (integrating the nutrient cycling in the water column), dissolved oxygen, Secchi depth, area-based biomass of benthic vegetation, as well as primary production. The model does not simulate zooplankton, which is not assumed as a state variable, but rather as a parameter of the phytoplankton processes (the phytoplankton grazing) (see Figure 2). The version used in this study did not simulate diagenesis (which corresponds to the biogeochemistry processes occurring at the interface between the water column and the upper layer of the bed sediments, see Figure 2), nor the suspended sediment dynamics of the water column, which results from the erosion, deposition and transport of sediments. The water turbidity, represented by the Secchi depth, corresponding to the water transparency, includes organic matter and detritus, inorganic matter, and suspended sediments (inputted from the boundaries), reflecting, therefore, the biogeochemical processes of the water column. The oxygen balance (DO) is an important issue, as it reflects the biogeochemical processes within the water column and the sediment layer, as well as the physical changes in the environment. The oxygen is produced by the primary producers and the benthic vegetation and the exchanges between the water/air interface, i.e., reaeration. Its consumption is due to the mineralization of organic matter in water and sediment, the ammonia oxidation (nitrification), and the respiration of zooplankton and phytoplankton. The mathematical formulations of the biological and chemical processes and transformations for each state variable are described by first-order ordinary and coupled differential equations that represent the mass balance within the water column and the sediment layer. Figure 2 summarises the conceptual diagram of the eutrophication model.
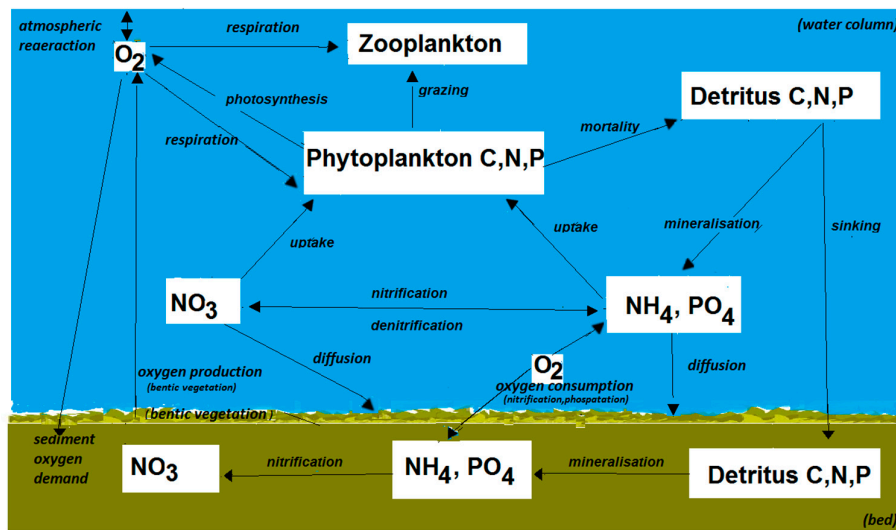
Figure 2. The conceptual diagram for the eutrophication model.

Dias et al. [47–50] implemented and assessed the hydrodynamic, salt, and heat transport models for the lagoon and showed the models can simulate and accurately reproduce the main pattern of the sea surface elevation, the current velocities, the salinity, and the water temperature, even in extreme meteorological conditions, constituting, therefore, a valuable tool for simulating and projecting physical changes under different forcings. The hydrodynamic and the transport models' calibration and the validation procedure were carried [49,50] out by comparing measured and predicted time series of the sea surface elevation (11 stations), current velocities (10 stations), salinity, and water temperature (6 stations) for the lagoon stations (11 stations). The results indicated that the hydrodynamic, salt, and heat transport models for Ria de Aveiro were successfully calibrated and validated, with accurate values for the root mean square errors (RMSE) for the hydrodynamic: <5% for sea surface elevation and higher values for the velocity, about 7%. The salinity and the water temperature validations were achieved for *RMSE* values ranging from 4% to about 9% for the former, and from 7% to about 17% for the latter. Concerning the eutrophication model, the validation was performed by comparing model predictions with observation data for the carbon phytoplankton and the chlorophyll-a, and for 7 stations [58,59], considering mean river flows and typical nutrient and suspended concentration values imposed at the river boundaries [56–60,62]. Data [56–60,62] suggest that nutrient concentrations inside the lagoon respond to the main constrains imposed at the river boundaries and small dependency on diagenesis. Up to now, no study has assessed the role of these processes in the nutrient dynamic of the lagoon. Concerning the carbon phytoplankton and the chlorophyll-a, Lopes et al. [58,59] showed that the model was able to reproduce data for the main lagoon stations. The RMSE errors calculated were below 10%, except for some discrepancies (~20–35%) for some stations, where the model failed to reproduce data.

3.2. The Scenarios Definition

The present study deals with the SLR scenarios at the lagoon coastal water. The scenarios have the purpose of quantifying the changes induced on the salinity, the temperature, and the biogeochemical state variables, relative to the baseline scenario (BS), which represents a typical late summer situation, but considering mean river discharges, as defined in Section 2. It is a realistic situation for the lagoon, which defines a clear ocean/river gradient distribution for the state variables, namely the salinity, as will be verified in Section 4.2. September 2000 was, therefore, selected as it represents a typical late summer lagoon situation, characterised by low river discharges, high range of salinity values (>30 PSU), and a well-defined temperature distribution, corresponding to low water temperature values near the lagoon

mouth (~17 °C) and high values at the inner areas (~ 20 °C). Furthermore, it is a period for which the nutrient concentrations were significantly high.

Tides and river discharges are the main forcings that determine significant changes in the physical and biogeochemical state variables. Tides were imposed at the ocean open boundary with the help of the Admiralty method of the Mike3 tide prediction of height [38], using the more recent harmonic constants for the tidal constituents for the lagoon entrance [34], which more accurately reflects changes in both the lagoon and coastal geomorphologies, which occurred during past decades. Mean river flows were imposed at the open river boundaries following the values defined in Section 2 and presented in Table 1. The initial and the boundary conditions for the physical and the biogeochemical state variables were set according to data from ModelRia [62] and defined in Tables 1 and 2, where the latter presents maximum and minimum values of the biogeochemical state variables for the main lagoon stations, as observed for September 2000. The interaction with the atmosphere is allowed at the surface, enabling the exchange of momentum and energy. The wind speed and velocity, the air temperature and humidity, the incident radiation and the sky clearness were imposed according to data from ModelRia [62].

The main objective of this study is to assess the impact of SLR on the ecosystem status of the lagoon water column, including the changes in the amplitude of the M2 tidal constituent (M2R), the river discharges (under *SLR)*, and the influence of a warming climate at the lagoon coastal area.

To define the scenarios, the following assumptions were made. Since global warming of at least 1.5–2 °C is now consensual for the future climate [2], 2 °C is, therefore, adopted as the value of the air temperature increase for a warmer climate scenario. Furthermore, concerning the trend of the mean sea level was, the following was adopted: global MSL has increased during the past century by approximately 200 mm [4], and it is very likely that it will rise by at least another 130 mm [8–15]. In particular, for the Portuguese coast (which includes the Ria de Aveiro [16,17]) a cumulated SLR of up to 0.75 m is likely for the year 2100, relative to the 1990 mean sea level [50], together with an increase of the M_2 component of the tide (up to 10%, [18–21]).

In view of the above considerations, Table 3 summarises the scenarios selected for this study, which will be developed in the next section.

The scenario SC1 (SLR/M2R) is based on BS and considers a future climate for which MSL rises by 1 m and the M_2 amplitude increases by 10%, while the river inflows remain unchanged relatively to BS conditions. Although this is the highest value of the projections for the MSL scenario for the study area, it is a very plausible situation considering the worst climate scenario. While SC2 (mean SLR/dry summer) represents an extreme event situation corresponding to a very dry summer for which the river discharges were set to a low limit or a residual value (10% of the reference values of BS), SC3 (warm climate scenario) simulates the warm climate at the lagoon coastal area, under SLR, for which the air temperature is 2 °C higher than the value for BS. This is also a scenario with a high degree of confidence, considering 2018 IPCC projections [1]. Furthermore, no changes in the initial and the boundary conditions values for the biogeochemical state variables were considered for the scenarios SC1, SC2, and SC3, when compared to BS. Due to the important *N/P* ratio, as presented in Section 2, nitrogen may be considered as the phytoplankton growth-limiting factor for the lagoon. For this reason, only results concerning nitrogen will be considered, although the role of *P* in the phytoplankton processes is non-negligible.

Table 1. The model boundary conditions, according to data [56–61].

Boundary	Mean Flow (m³/s)	Salinity (PSU)	Temperature (°C)	Inorganic Nitrogen Concentration (mg/L)	Nitrogen Total [1] Concentration (mg/L)	PC [2] (mg/L)	DO [3] (mg/L)	Seston [4] (mg/L)
Antuã	10	0	20	0.6	7.2	0.3	7.8	3.7
Boco	5	0	20	-	3.4	0.2	9.5	22.2
Caster	5	0	20	2.2	9.9	0.2	9.4	3.4
Mira	10	0	20	1.3	2.0	0.5	8.2	22.8
Vouga	50	0	20	0.7	1.9	0.4	7.5	12.9
Ocean	-	35	17	0.1	-	0.2	10.0	0.1

[1] Includes organic and inorganic nitrogen; [2] concentration of carbon phytoplankton; [3] concentration of dissolved oxygen; [4] Seston refers to suspended particulate matter in the water column, including plankton, nekton and other organic matter.

Table 2. Observed maximum and minimum values for the physical and biogeochemical state variables and for the main lagoon stations, for September 2000, according to data [56–60,62].

Stations		Salinity (PSU)	Temperature (°C)	Secchi [1] Depth (m)	Inorganic Nitrogen Concentration (mg/L)	PC (mg/L)
St1	Minimum	32.5	17.9	2	0.1	0.2
	Maximum	35.1	20.8	-	0.1	0.2
St2	Minimum	33.6	18.9	1.7	0.1	1
	Maximum	34.4	20.2	-	0.2	0.2
St3	Minimum	32.7	19.6	1.3	0.2	0.4
	Maximum	33.8	20.4	-	1.3	0.4
St4	Minimum	(0.7)30.0 [2]	19.8	-	1.2	0.4
	Maximum	(0.7)30.0 [2]	20.6	-	1.3	0.4
St5	Minimum	34.1	18.4	1.9	0.1	0.2
	Maximum	34.7	19.2	-	0.2	0.3
St6	Minimum	32.5	20.1	-	0.2	0.2
	Maximum	34.4	21.0	-	0.3	0.3
St7	Minimum	29.2	20.2	-	0.1	0.2
	Maximum	30.2	22.3	-	0.1	0.3

[1] Secchi depth: measure the visibility of the water column, in depth (m). [2] Observations performed at two different points, near the river boundary.

Table 3. The scenarios description, combining the effects of, the sea level rise, SLR, the M_2 amplitude, the river discharge and the air temperature.

Scenarios [1]	SLR [2]	ΔM_2 [3]	ΔAirT [4]	River Discharges
BS	0 m	0	0	Mean river flow
SC1	+1 m	+10%	0	Mean river flow
SC2	+1 m	+10%	0	10% Mean river flow
SC3	+1 m	+10%	2 °C	Mean river flow

[1] BS—baseline; SC1—SLR/M2R; SC2—SLR/M2R and dry summer; SC3—SLR/ M2R and warm climate [2] SLR—sea level rise; [3] ΔM_2—variation of the amplitude of the M_2 component of the tide (M2R); [4] ΔAirT —variation of the air temperature.

To compare results between the time series of two scenarios, SCI and SCJ, it was calculated at each instant the difference between them, defined as: $\Delta(V) = V(SCI)-V(SCJ)$, where V represents a given model output variable (salinity, temperature, etc). This parameter was computed for different scenarios and model outputs. To graphically compare the model outputs, Taylor diagrams [64] were constructed. They usually assess a model's skill to simulate the reality by comparing a model output to observation. It is performed by statistically quantifying their 'proximity', while the results are graphically displayed in a diagram containing the main statistical metrics. It requires the computation of the correlation between the scenarios and the baseline simulation, as well as their centered root-mean-square difference:

$$R = \frac{\frac{1}{N}\sum_{n=1}^{N}\left(f_n - \overline{f}\right)(r_n - \overline{r})}{\sigma_f \sigma_r}$$

$$E'^2 = \frac{1}{N}\sum_{n=1}^{N}\left\{\left(f_n - \overline{f}\right)(r_n - \overline{r})\right\}^2$$

$$\sigma_f^2 = \frac{1}{N}\sum_{n=1}^{N}\left(f_n - \overline{f}\right)^2$$

$$\sigma_r^2 = \frac{1}{N}\sum_{n=1}^{N}(r_n - \overline{r})^2$$

where "R" and "E'" represent, respectively, the Pearson correlation coefficient and the centered root-mean-square deviation RMSD between the simulation time-series (noted as "f") and the baseline/reference time series (noted as "r"), and σ_f and σ_r the standard deviations of the simulation field and of the baseline/reference field, respectively.

4. Results

This section presents the results of the climate change scenarios, as defined in Table 3. It addresses the influence of changes of the mean sea level and the amplitude of the M_2 component of the tide, the freshwater discharge, and the effect of warm climate in the lagoon water column.

4.1. The Mean Sea Level Rise (MSLR) Scenario, (SC1)

This section deals exclusively with results concerning BS and SC1.

Figures 3 and 4 present the salinity and the δ(salinity) time series for BS, SC1 and SC2, and the lagoon stations, defined in Figure 1 and covering a late summer situation (September 2000). Table 4 presents the statistic metrics for Δ(Salinity) (maximum, minimum, mean values, and standard deviation), representing the difference between the two time series, with BS corresponding to SCI and SC1 or SC2 corresponding to SCJ. RIFEN will be used as abbreviation when referring to major rivers (St3 and St4) and far end areas (St6, St7, and St8).
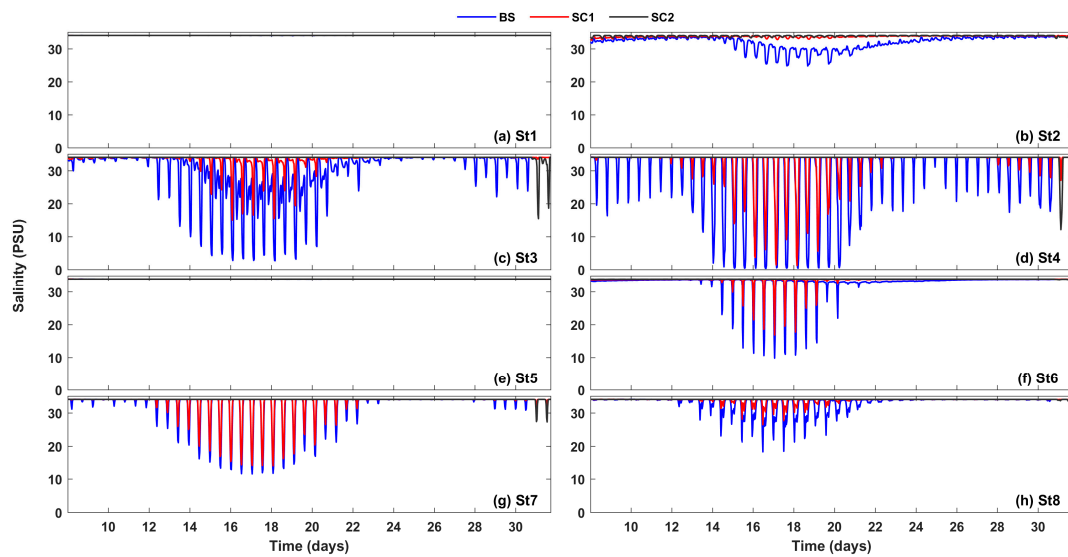
Figure 3. Time series of salinity for the scenarios BS, SC1 and SC2, for September 2000, and the lagoon stations: (**a**) St1, (**b**) St2, (**c**) St3, (**d**) St4, (**e**) St5, (**f**) St6, (**g**) St7 and (**h**) St8.
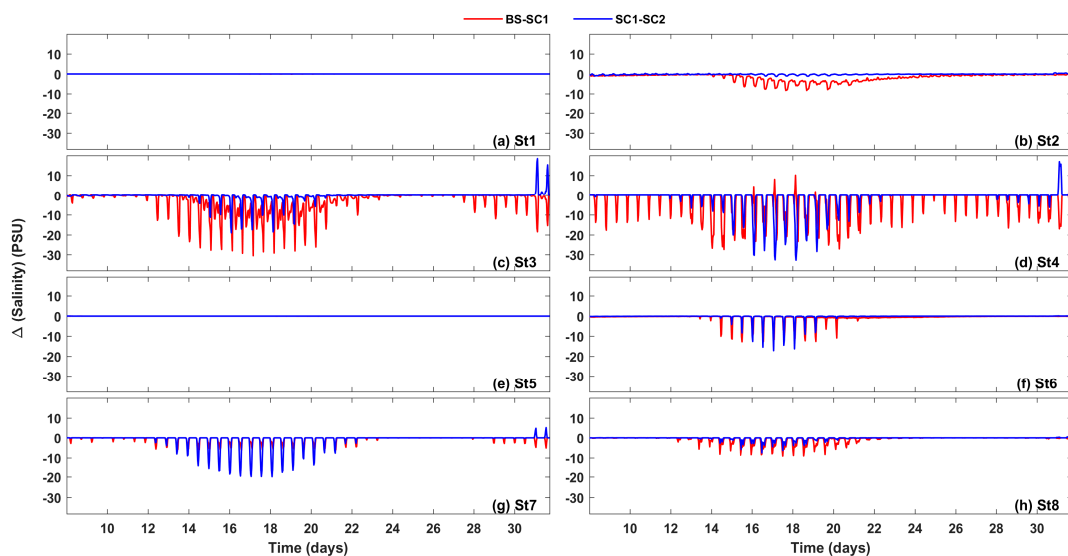
Figure 4. Time series of the salinity difference, Δ(Salinity), between the scenarios (BS–SC1, SC1–SC2), for September 2000, and the lagoon stations: (**a**) St1, (**b**) St2, (**c**) St3, (**d**) St4, (**e**) St5, (**f**) St6, (**g**) St7 and (**h**) St8.

It can be observed that the salinity time series are characterised by the tidal cycle, which is semi-diurnal, with strong spring-neap tide modulation. Except for the spring-neap period (12/9/2000 to 23/9/2000), during which the salinity values oscillate between those of freshwater (~5 PSU) and those of the ocean water (~34 PSU), a situation which reflects the competing influence between the ebbing and the flooding flows, salinity presents, in general, typical values for the late summer (~34 PSU), close to the ocean water salinity, as observed in Table 2.

In particular, the RIFEN stations present during the spring and low tide, when the ebb flow is strong, important salinity oscillations, with values varying within a wide range ((5–34 PSU) or (15–34 PSU)), evidencing the competing influence between the river and the ocean waters. In particular, St2, situated near the lagoon mouth along the Espinheiro channel and connecting the main river (Vouga) and the ocean, reflects the river influence, as the salinity values oscillate between the ocean boundary values (~34 PSU) and the mix-water values (~25 PSU).

Table 4. Salinity difference, Δ(Salinity), metrics for BS–SC1 and SC1–SC2, and the lagoon stations (St1–St8).

Stations	Scenarios	Minimum Δ(Salinity) (PSU)	Maximum Δ(Salinity) (PSU)	Average Δ(Salinity) (PSU)
St1	BS–SC1	−0.08	0.04	−0.00
	SC1–SC2	−0.00	0.05	0.00
St2	BS–SC1	−8.30	−0.09	−1.63
	SC1–SC2	−1.24	0.28	−0.19
St3	BS–SC1	−30.54	0.10	−3.07
	SC1–SC2	−19.0	0.01	−0.57
St4	BS–SC1	−27.4	10.23	−3.00
	SC1–SC2	−32.8	0.00	−1.51
St5	BS–SC1	−0.04	0.04	0.00
	SC1–SC2	−0.00	0.00	0.000
St6	BS–SC1	−12.70	−0.04	−0.66
	SC1–SC2	−17.19	−0.00	−0.28
St7	BS–SC1	−6.44	0.02	−0.48
	SC1–SC2	−19.86	0.01	−0.94
St8	BS–SC1	−6.44	0.02	−0.48
	SC1–SC2	−7.58	0.02	−0.21

Concerning SC1, an overall increase of salinity is observed, which reflects the dominant influence of ocean water. Consequently, the RIFEN stations have shown a wide range of salinity values (15–34 PSU). On the other hand, St1, St2, and St5 show salinity values almost constant (~34 PSU), reflecting proximity to the ocean boundary (St1 and St2) or location along the S. Jacinto channel (St5). The time series of the salinity difference between BS and SC1, Δ(Salinity), (Figure 4), reflect the changes between the two scenarios. They present negative values for all stations (see Table 4, BS–SC1). While St1, St2, and St5 show the smallest values (|Δ(Salinity)|< 0.1 PSU), as the salinity (~34 PSU) does not present any significant variation between BS and SC1, the RIFEN stations present high amplitude oscillation, with |Δ(Salinity)| reaching high values (30 PSU (for St3), 25 PSU (for St4), 10–20 PSU (for St6, St7, and St8) and 8 PSU (for St2)) (see the minimum values in Table 4). Figure 5 presents snapshots of the surface distribution of salinity for BS (a), SC1 (b), and SC2 (c), for two moments: (1) high tide, flooding at the lagoon mouth and ebbing at the mouth of the rivers (2); high tide, ebbing at the lagoon mouth and flooding at the mouth of the rivers. Considering the SC1 snapshots, it can be observed that they represent a configuration of the lagoon almost filled with ocean water, as was apparent in the salinity time series. Indeed, during the spring-neap tide and flooding the ocean waters reach the RIFEN areas, their salinity reaching high values, while during the ebb period the salinity fronts did not displace very far from those areas and downstream toward the lagoon central areas. The scenario results evidence, therefore, the dominant influence of the ocean water on the lagoon salinity patterns, under the competing influence of the river and the ocean forcing.
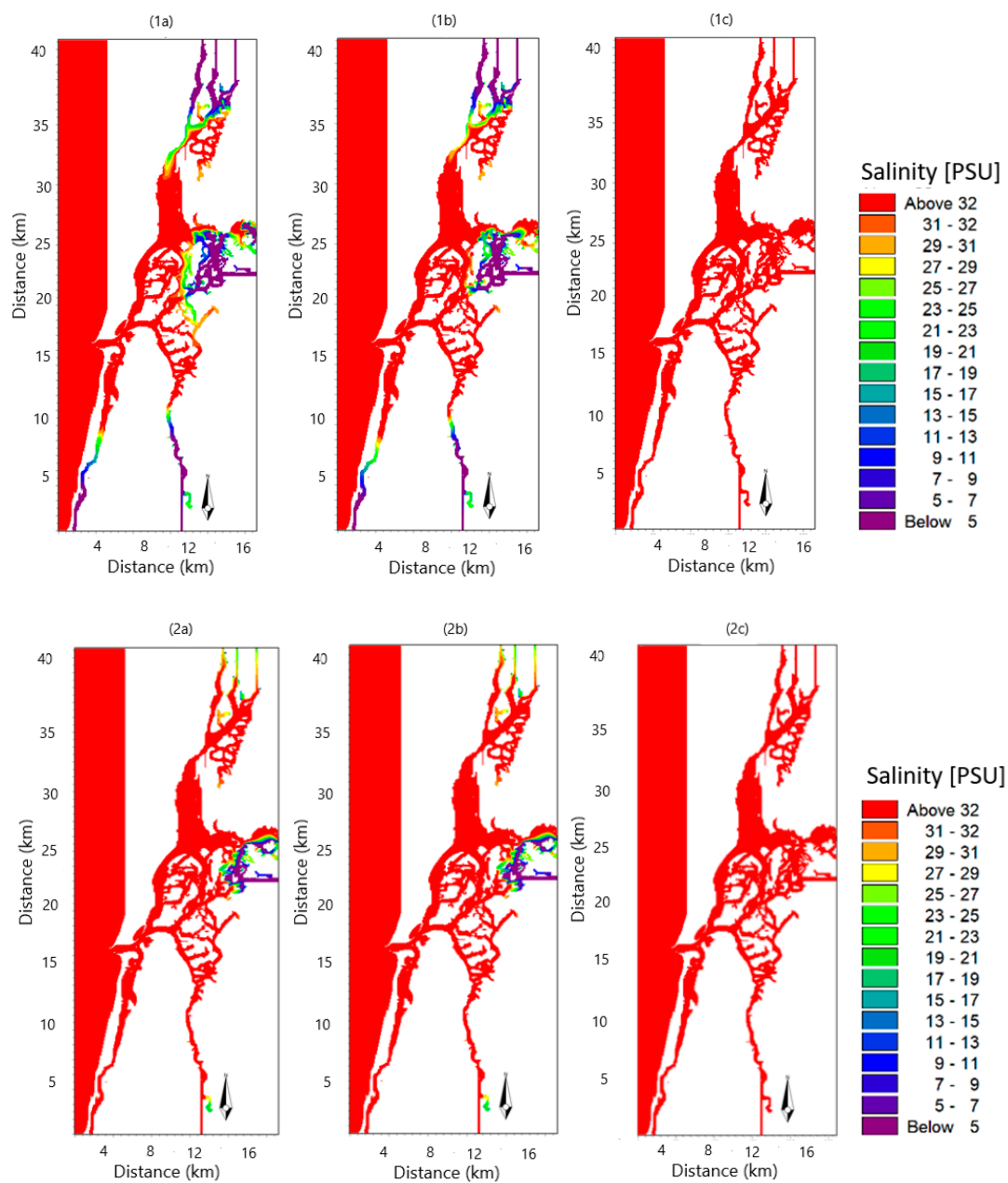
Figure 5. Snapshots of the surface salinity (PSU) for BS (**a**), SC1 (**b**), and SC2 (**c**), for two instants: 1—high tide, flooding at the lagoon mouth and ebbing at the mouth of the rivers (17/9/2000); 2—high tide, ebbing at the lagoon mouth and flooding at the mouth of the rivers (27/9/2000).

Figure 6 presents the water temperature time series, similar to Figure 4. They show typical diurnal patterns, with a spring-neap tide modulation, while the temperature values vary within the range of 18.5–21.5 °C (corresponding to the amplitude oscillation range ~1.5 °C). St1 shows the lowest temperature values, as well as the smallest range of variation, 18.5–19.6 °C, reflecting its location near the ocean boundary, while the RIFEN stations show the highest values and range of variation, 19–21.5 °C. On the other hand, SC1 shows significant water temperature decrease relatively to BS, for all the stations. Indeed, the water temperature difference between BS and SC1, Δ(Temperature), (Figure 7), presents positive values, ranging from 0.1 to 1 °C, as observed for the maximum and the average values (Table 5), while some negative values may be considered non-significant, as they may be associated with turbulent fluctuations. Figure 8 represents snapshots of the surface distribution of temperature, similar to Figure 5. During the spring-neap tide and flooding, due to the increase of the

ocean cold water flow into the lagoon, the ocean waters reach the RIFEN areas, leading to a decrease of the water temperature to values close to the ocean waters. As for the salinity, the results confirm the dominant influence of the ocean waters under the competing influence of the river and the ocean forcing. During the spring-neap tide and flooding, due to the increase of the ocean, cold water flows into the lagoon and reaches the RIFEN areas, leading to the water temperature decrease.
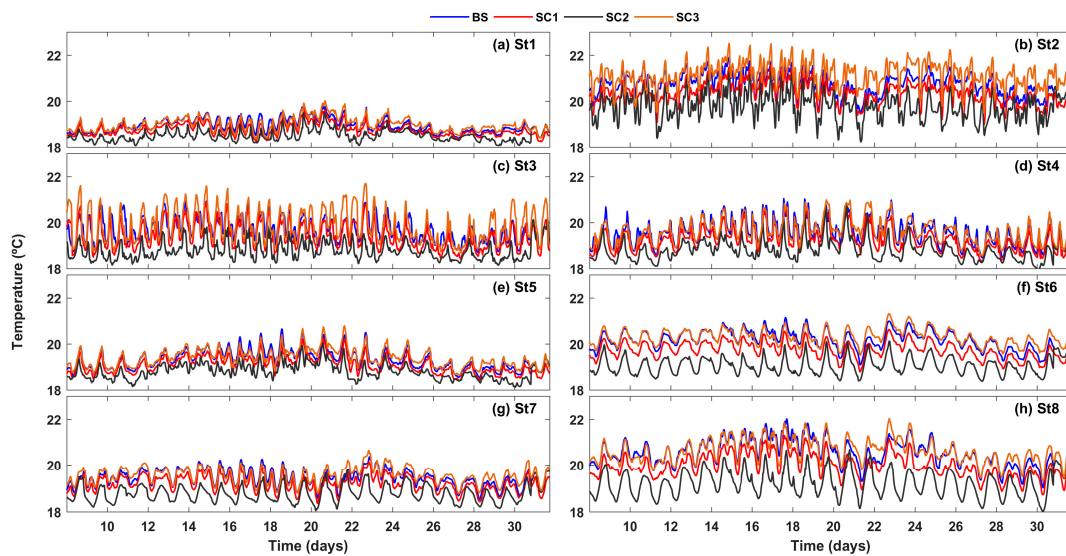
Figure 6. Time series of the water temperature for the scenarios, BS, SC1, SC2, and SC3, for September 2000, and the lagoon stations: (**a**) St1, (**b**) St2, (**c**) St3, (**d**) St4, (**e**) St5, (**f**) St6, (**g**) St7 and (**h**) St8.
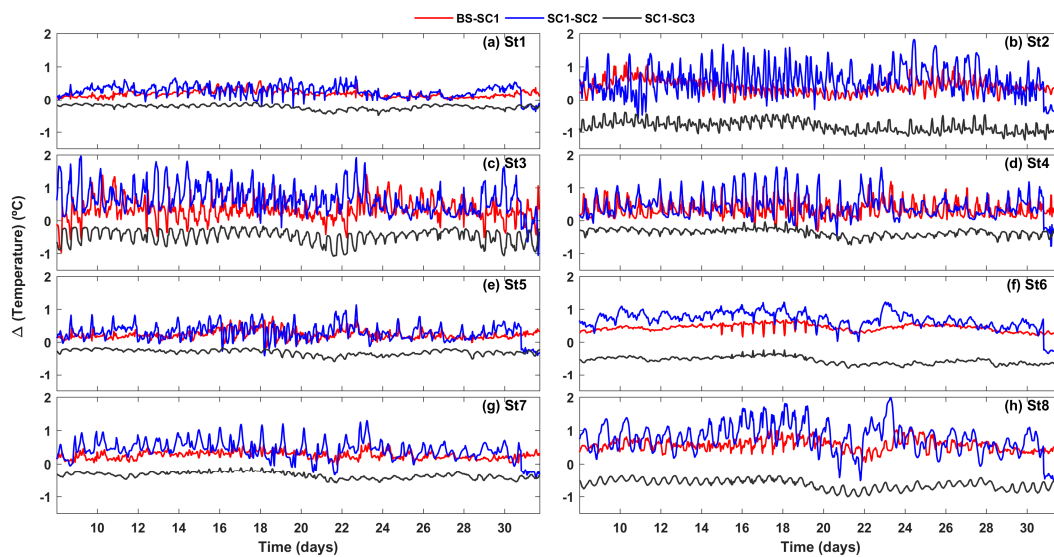
Figure 7. Time series of the water temperature difference, Δ(Temperature), between the scenarios (BS–SC1, SC1–SC2 and SC1–SC3), for September 2000, and the lagoon stations: (**a**) St1, (**b**) St2, (**c**) St3, (**d**) St4, (**e**) St5, (**f**) St6, (**g**) St7 and (**h**) St8.

The next figures present time series for the following biogeochemical variables: the inorganic nitrogen (IN), the carbon phytoplankton (PC), and the Secchi depth (ScD), for the baseline (BS) and the scenario simulations (SC1 and SC2), but, again, only the results of BS and SC1 are considered in this section.

Table 5. Water temperature difference (Δ(Temperature)) metrics for BS–SC1 and SC1–SC2, and the lagoon stations (St1–St8).

Stations	Scenarios	Minimum Δ(Temperature) ($^\circ$ C)	Maximum Δ(Temperature) ($^\circ$ C)	Average Δ(Temperature) ($^\circ$ C)
St1	BS–SC1	−0.03	0.58	0.18
	SC1–SC2	0.20	0.70	0.24
St2	BS–SC1	−0.40	1.14	0.38
	SC1–SC2	0.05	1.90	1.00
St3	BS–SC1	−0.96	1.40	0.29
	SC1–SC2	−1.33	1.77	0.26
St4	BS–SC1	−0.33	1.19	0.33
	SC1–SC2	−0.91	1.45	0.25
St5	BS–SC1	−0.16	0.078	0.22
	SC1–SC2	−0.21	1.02	0.28
St6	BS–SC1	0.16	0.68	0.43
	SC1–SC2	−0.05	1.20	0.70
St7	BS–SC1	−0.5	0.62	0.25
	SC1–SC2	−0.46	1.20	0.29
St8	BS–SC1	−0.13	1.06	0.54
	SC1–SC2	−0.9	1.46	0.41

Figure 9 presents IN time series similar to Figure 4. They evidence tidal patterns (semi-diurnal) with spring neap-tide modulation. In general, the inorganic nitrogen concentration values, IN, vary within the range of 0.5–2 mg L^{-1}, which are typical for the lagoon, as observed in Table 6. In particular, the RIFEN stations show the highest concentration values (~2 mg L^{-1}), which are reached during the spring tide, evidencing the influence of the nutrient discharged at the river boundaries, while St1 and St5, which are located close to the ocean boundary and along the S. Jacinto channel, respectively, show the lowest values (<1 mg L^{-1}). On the other hand, *BS* and *SC1*, show significant differences between the RIFEN stations, namely during the spring tide. Indeed, it can be observed that the time series of the inorganic nitrogen concentration difference Δ(IN) between BS and SC1 (Figure 10) show positive values, the maximum values reaching 2 mg L^{-1} (Table 6), corresponding to an overall reduction of the IN concentrations for SC1 relatively to BS. Under the scenario, the increase of the flow of ocean IN-poor water into the lagoon, leads, therefore, to an overall drop of the inorganic nitrogen concentration. Indeed, Figure 11, which represents snapshots of the surface distribution of the inorganic nitrogen concentration, confirms that the fronts between the river's inorganic nitrogen-rich waters and the lagoon mix-waters are pushed far ahead toward the lagoon far ends.
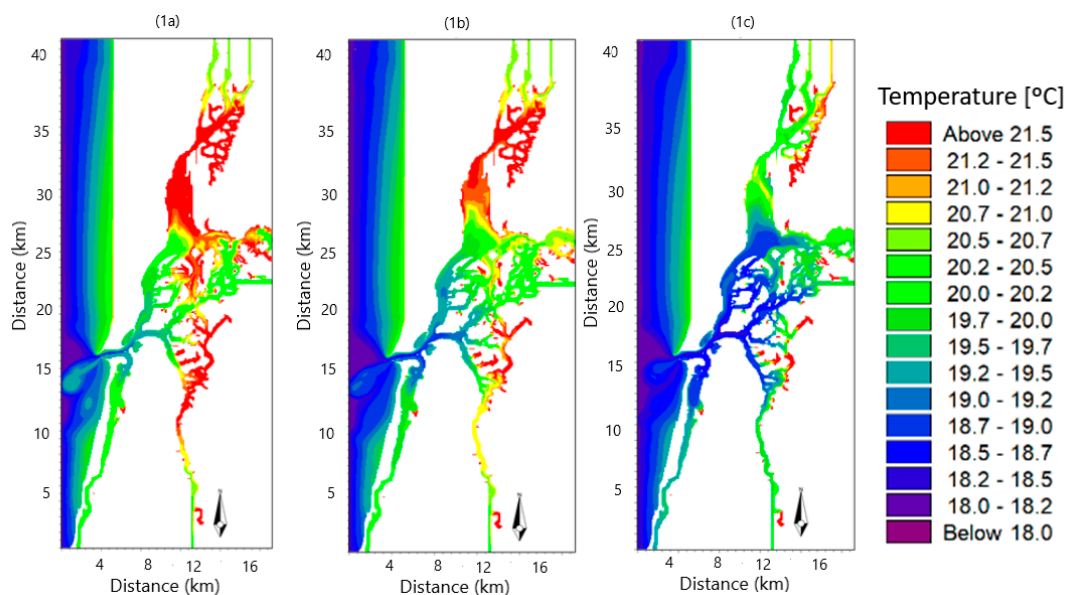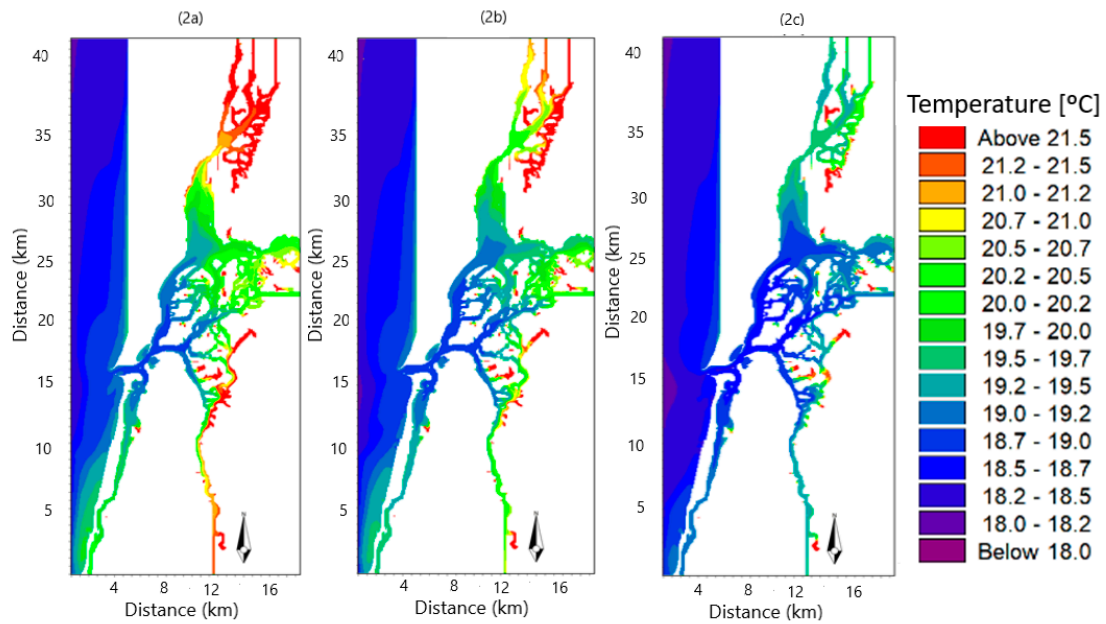

Figure 8. *Cont.*

Figure 8. Snapshots of surface temperature (°C) for BS (**a**), SC1 (**b**), and SC2 (**c**), for two instants: 1—high tide, flooding at the lagoon mouth and ebbing at the mouth of the rivers (17/9/2000); 2—high tide, ebbing at the lagoon mouth and flooding at the mouth of the rivers (27/9/2000).

Table 6. Inorganic nitrogen concentration difference, Δ(IN), metrics for BS–SC1 and SC1–SC2, and the lagoon stations (ST1–ST8).

Stations	Scenarios	Minimum Δ(IN) (mg L^{-1})	Maximum Δ(IN) (mg L^{-1})	Average Δ(IN) (mg L^{-1})
St1	BS–SC1	−0.1	0.32	0.05
	SC1–SC2	−0.17	0.34	−0.07
St2	BS–SC1	−0.51	1.13	0.33
	SC1–SC2	0.60	2.07	0.32
St3	BS–SC1	1.00	1.66	0.18
	SC1–SC2	−0.18	1.72	0.24
St4	BS–SC1	−0.64	1.46	0.24
	SC1–SC2	−0.16	1.91	0.19
St5	BS–SC1	−0.16	0.39	0.05
	SC1–SC2	−0.20	0.57	0.07
St6	BS–SC1	0.00	1.13	0.25
	SC1–SC2	−0.09	1.40	0.20
St7	BS–SC1	−0.02	0.50	0.90
	SC1–SC2	−0.11	1.12	0.13
St8	BS–SC1	0.023	2.38	0.28
	SC1–SC2	−0.11	1.41	0.22
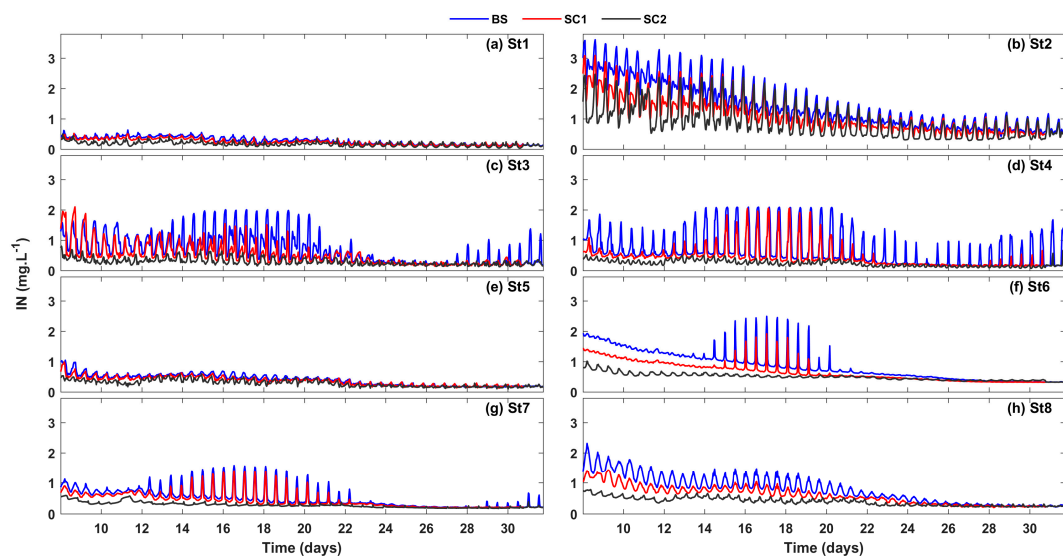
Figure 9. Time series of the inorganic nitrogen concentration (IN), for the scenarios, BS, SC1 and SC2, for September 2000, and the lagoon stations: (**a**) St1, (**b**) St2, (**c**) St3, (**d**) St4, (**e**) St5, (**f**) St6, (**g**) St7 and (**h**) St8.
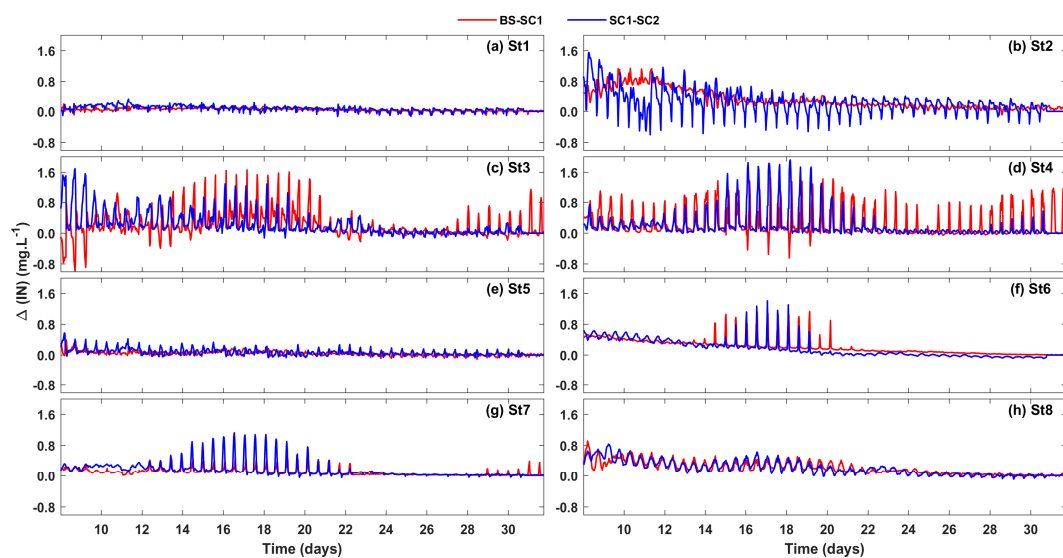

Figure 10. Time series of the inorganic nitrogen concentration difference, Δ(IN), between the scenarios (BS–SC1 and SC1–SC2), for September 2000, and the lagoon stations: (**a**) St1, (**b**) St2, (**c**) St3, (**d**) St4, (**e**) St5, (**f**) St6, (**g**) St7 and (**h**) St8.

Figure 12 presents the Secchi depth, ScD, time-series similar to Figure 4. It can be observed that the values are typical for the lagoon waters, as in Table 2. While the RIFEN stations show values within a wide range (0.6 m–1.8 m) and the lowest values, the remaining stations show a tighter range (~1.2 m–1.8 m) or (~1.6 m–1.8 m). On the other hand, St1, St2, and St5, located close to the ocean boundary and along the S. Jacinto channel, respectively, always show high values (>1.2 m). The major oscillations are found during the spring tide period. Considering the scenario SC1, it can be observed that St2 and the RIFEN stations show a significant reduction of the ScD values during the spring tide period, reaching values as low as 0.6 m. Indeed, Δ(ScD) time series (Figure 13) show, in general, negative values, namely at the RIFEN stations, where Δ(ScD) reaches values as low as −1 m (see Table 7). The scenario highlighted, therefore, the relative importance of the ocean and the rivers waters in the ScD patterns. Indeed, during the spring tide and ebbing, the river waters flow toward the central

areas of the lagoon, contributing, therefore, to a decrease of ScD, while the ocean flow has an opposite effect, carrying transparent waters into the lagoon. Although the greater shear the flow may generate, this effect cannot, in the present version of the model, potentially increase the turbidity of the water column and reduce the Secchi depth through the resuspension of sediment, as the model does not address the sediment processes of the water column integrating the interaction with the sediment bed (erosion and deposition). The turbidity is generated by both rivers inputting suspended organic and inorganic matter and the biogeochemical processes generated in the water column. It is worth noting that the ScD fronts between the river waters and the lagoon mix-waters remain localized close to the lagoon far ends, as can be observed in Figure 14, which represents the snapshots of the Secchi depth distribution.
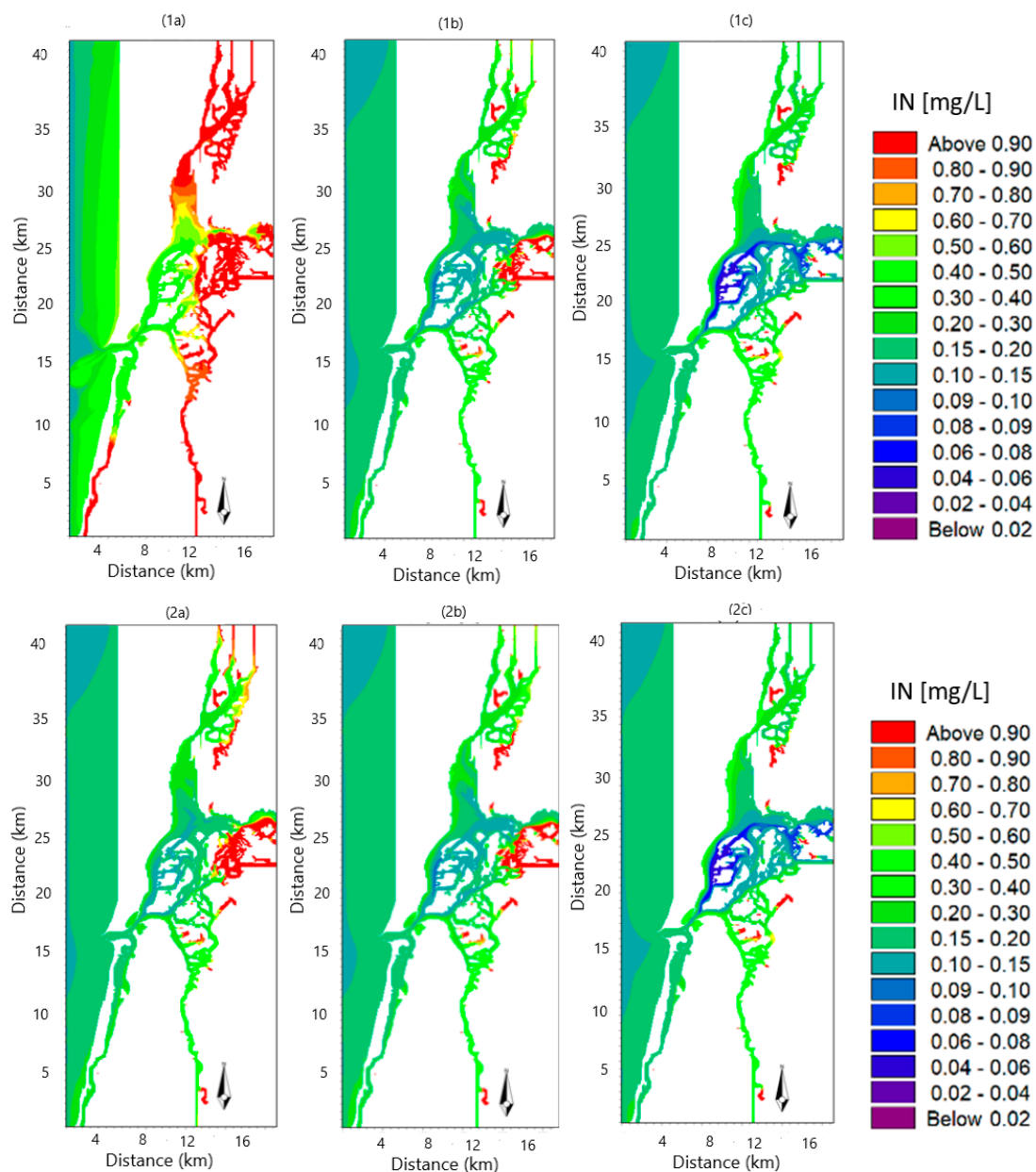
Figure 11. Snapshots of surface concentration of inorganic nitrogen, IN, for BS (**a**), SC1 (**b**), and SC2 (**c**), for two instants: 1—high tide, flooding at the lagoon mouth and ebbing at the mouth of the rivers (17/9/2000); 2—high tide, ebbing at the lagoon mouth and flooding at the mouth of the rivers (27/9/2000).
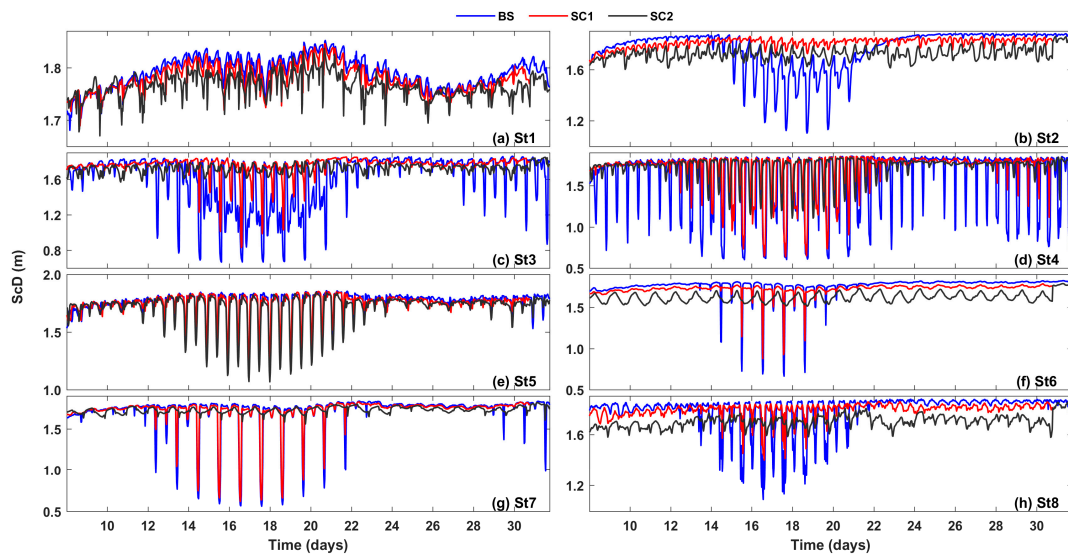
Figure 12. Time series of the Secchi depth, ScD, for the scenarios, BS, SC1 and SC2, for September 2000, and the lagoon stations: (**a**) St1, (**b**) St2, (**c**) St3, (**d**) St4, (**e**) St5, (**f**) St6, (**g**) St7 and (**h**) St8.
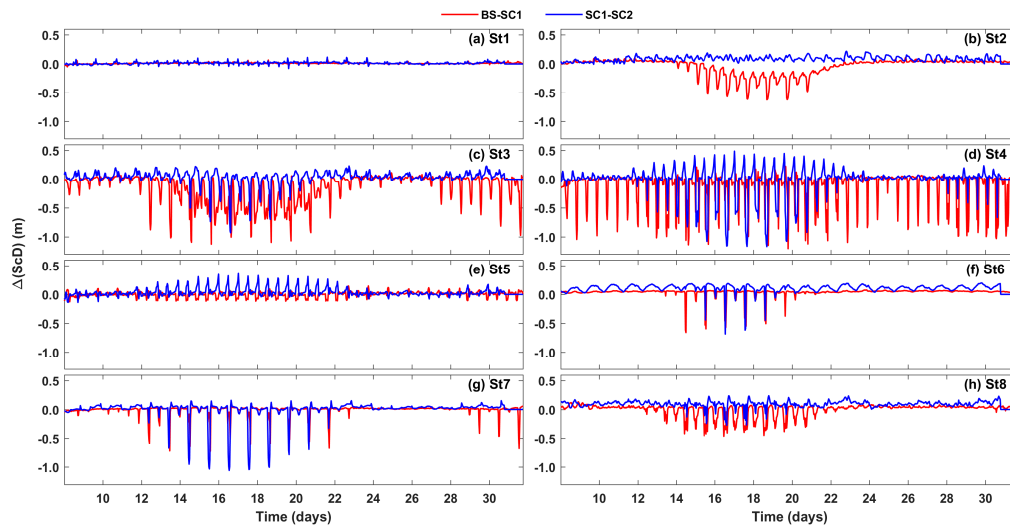

Figure 13. Time series of the Secchi depth difference, Δ(ScD), between the scenarios (BS–SC1 and SC1–SC2), for September 2000, and the lagoon stations: (**a**) St1, (**b**) St2, (**c**) St3, (**d**) St4, (**e**) St5, (**f**) St6, (**g**) St7 and (**h**) St8.

Table 7. Secchi depth difference, Δ(ScD), metrics for BS–SC1 and SC1–SC2, and the lagoon stations (St1–St8).

| Stations	Scenarios	Minimum Δ(ScD) (m)	Maximum Δ(ScD) (m)	Average Δ(ScD) (m)
St1	BS–SC1	−0.063	0.05	−0.04
	SC1–SC2	−0.05	0.18	0.01
St2	BS–SC1	−1.13	0.12	0.14
	SC1–SC2	−0.44	0.22	0.07
St3	BS–SC1	−1.21	0.23	−0.14
	SC1–SC2	−0.93	0.23	0.03
St4	BS–SC1	−1.15	0.15	0.00
	SC1–SC2	−1.16	0.45	−0.02
St5	BS–SC1	−0.70	0.08	0.03
	SC1–SC2	−0.07	0.36	0.10
St6	BS–SC1	−0.74	0.06	−0.01
	SC1–SC2	−0.68	0.20	0.09
St7	BS–SC1	−0.65	0.13	−0.02
	SC1–SC2	−1.06	0.16	−0.00
St8	BS–SC1	−0.16	0.09	0.01
	SC1–SC2	−0.27	0.24	0.09
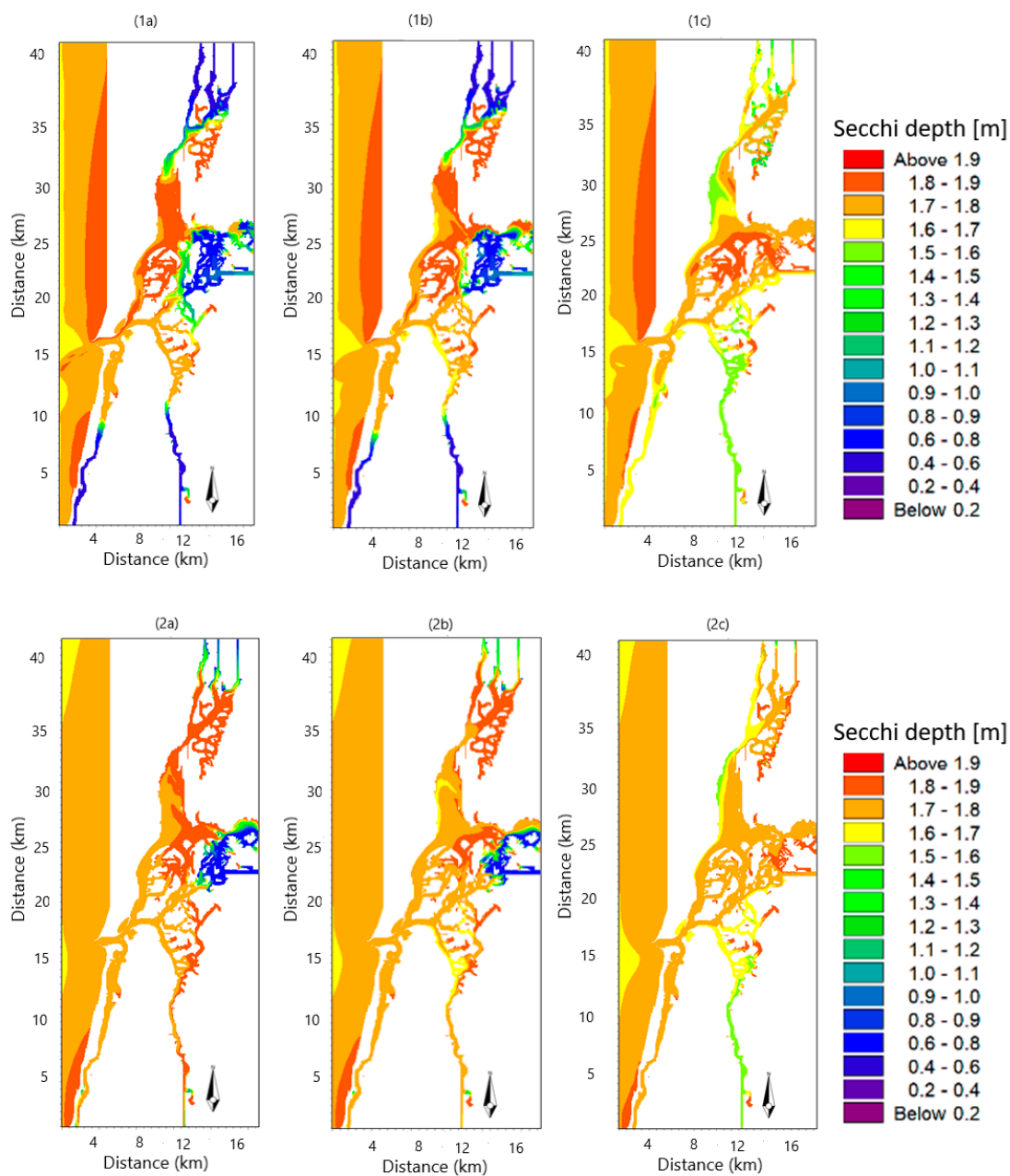
Figure 14. Snapshots of Secchi depth, ScD, for BS (**a**), SC1 (**b**), and SC2 (**c**), for two instants: 1—high tide, flooding at the lagoon mouth and ebbing at the mouth of the rivers (17/9/2000); 2—high tide, ebbing at the lagoon mouth and flooding at the mouth of the rivers (27/9/2000).

The carbon phytoplankton concentration, PC, time series (Figure 15) show typical values for the lagoon, as observed in Table 2, evidencing the relationship between phytoplankton and nutrients (IN). Indeed, it follows the same trend as IN, as it shows namely an important increase in concentration during the spring tide period. It is worth noting that St2 and the RIFEN stations show the highest concentration values (~0.3 mg L^{-1} and 0.5 mg L^{-1}, respectively) during the spring tide period, while St1 and St5 show no significant variations and the smallest values (~0.1 mg L^{-1}). Δ(PC) time series (Figure 16) show significant and positive values, namely during the spring tide period, reflecting the concentration decrease for SC1 relatively to BS, as can be observed from the high maximum values (>0.4 mg L^{-1}) for the RIFEN stations (see Table 8). Indeed, during this period, SC1 still experience a phytoplankton bloom, as observed for BS. The results are coherent with those observed for the salinity and the water temperature, IN and ScD, as, under the scenario, the increasing of the ocean

inflow brings nutrient-poor water into the lagoon, leading, therefore, to an overall decrease of IN and, consequently, a reduction of phytoplankton growth. Figure 17(1b,2b), which represents snapshots of the surface distribution of the carbon phytoplankton concentration, shows that under SC1 the phytoplankton bloom, which is set up at the RIFEN areas, as observed for BS, is pushed ahead toward the far ends. This result is not surprising, as previously observed results show, as under the scenario, the increasing of the ocean inflow brings nutrient-poor water into the lagoon, leading, therefore, to an overall decrease of IN and, consequently, to the reduction of phytoplankton growth, provided that there is no condition for IN-limited growth.
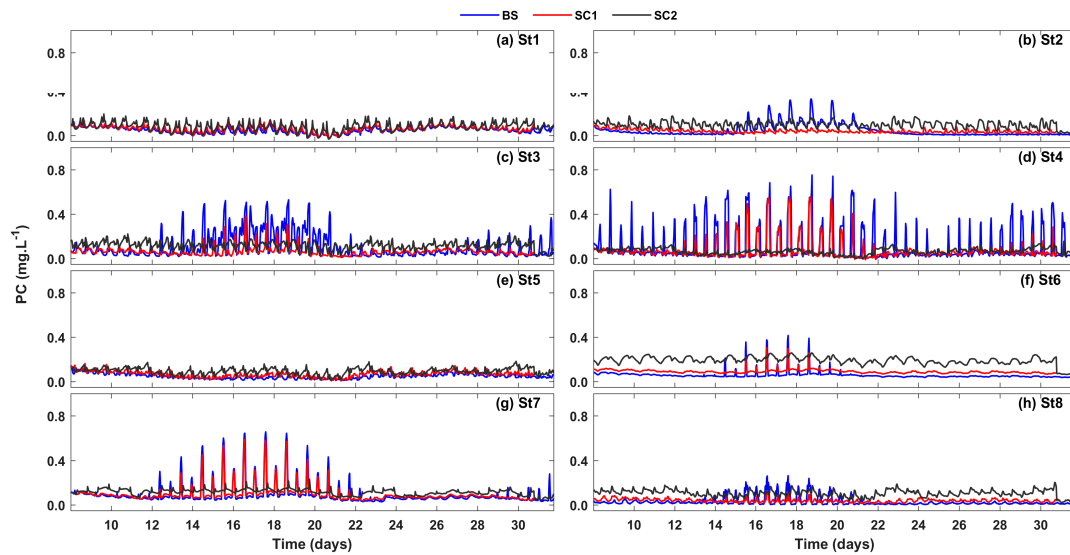
Figure 15. Time series of the carbon phytoplankton concentration, PC, for the scenarios, BS, SC1, and SC2, for September 2000, and the lagoon stations: (**a**) St1, (**b**) St2, (**c**) St3, (**d**) St4, (**e**) St5, (**f**) St6, (**g**) St7 and (**h**) St8.
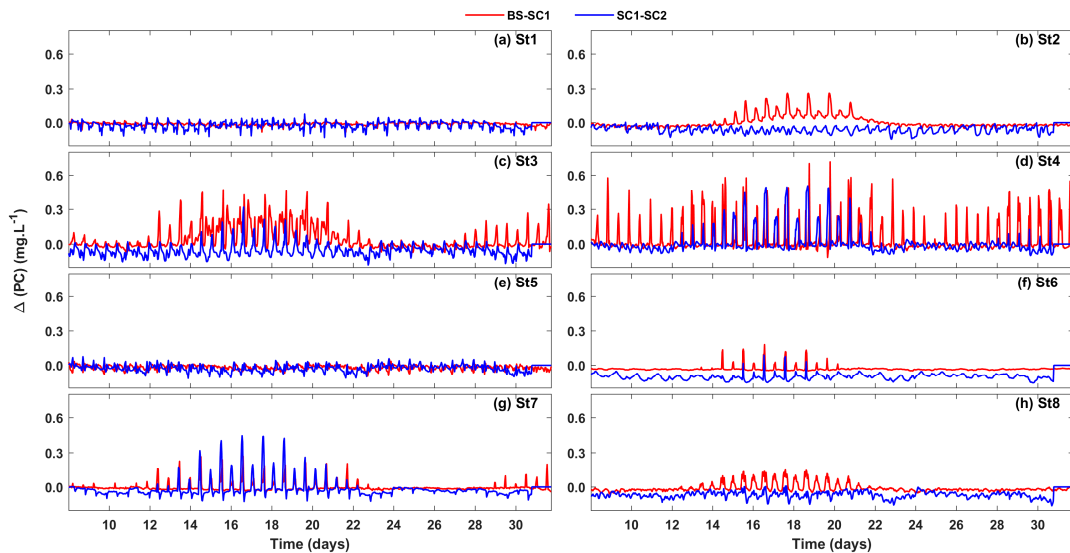

Figure 16. Time series of carbon phytoplankton concentration difference, Δ(PC), between the scenarios (BS–SC1 and SC1–SC2), for September 2000 and the lagoon stations: (**a**) St1, (**b**) St2, (**c**) St3, (**d**) St4, (**e**) St5, (**f**) St6, (**g**) St7 and (**h**) St8.

Table 8. Carbon phytoplankton concentration difference, Δ(PC), metrics for BS–SC1 and SC1–SC2, and the lagoon stations (St1–St8).

Stations	Scenarios	Minimum Δ(PC) mg L^{-1}	Maximum Δ(PC) mg L^{-1}	Average Δ(PC) mg L^{-1}
St1	BS–SC1	−0.08	0.05	−0.01
	SC1–SC2	−0.13	0.06	−0.03
St2	BS–SC1	−0.07	0.26	0.01
	SC1–SC2	−0.16	0.20	−0.05
St3	BS–SC1	−0.07	0.47	0.05
	SC1–SC2	−0.20	0.48	−0.01
St4	BS–SC1	−0.12	0.73	0.05
	SC1–SC2	−0.10	0.50	0.05
St5	BS–SC1	−0.10	0.05	−0.02
	SC1–SC2	−0.16	0.05	−0.05
St6	BS–SC1	−0.05	0.18	−0.03
	SC1–SC2	−0.20	0.20	−0.13
St7	BS–SC1	−0.04	0.27	−0.00
	SC1–SC2	−0.15	0.51	−0.02
St8	BS–SC1	−0.05	0.2	−0.01
	SC1–SC2	−0.20	0.16	−0.07
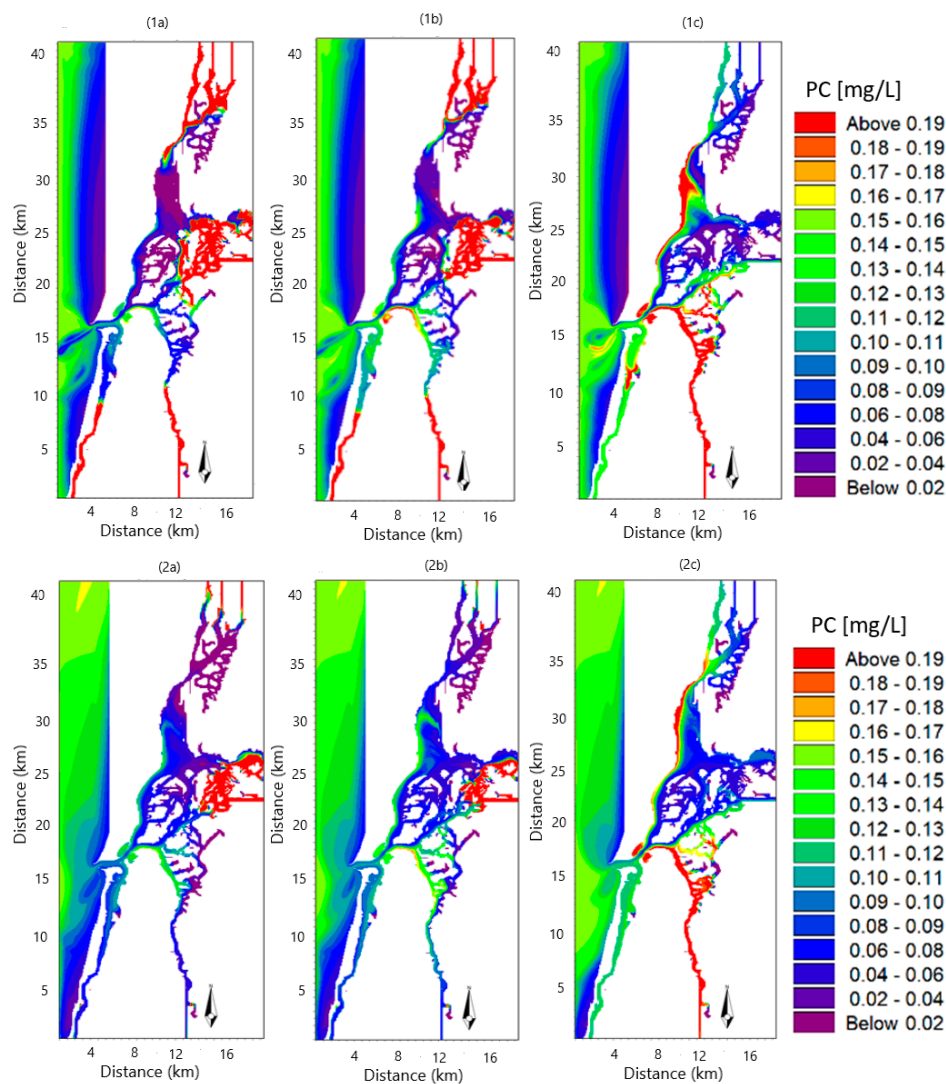
Figure 17. Snapshots of surface concentration of carbon phytoplankton, PC, for BS (**a**), SC1 (**b**) and SC2 (**c**), for two instants: 1—high tide, flooding at the lagoon mouth and ebbing at the mouth of the rivers (17/9/2000); 2—high tide, ebbing at the lagoon mouth and flooding at the mouth of the rivers (27/9/2000).

4.2. The Mean Sea Level Rise (MSLR) and Dry Summer Situation Scenario (SC2)

In this section, it was found to be more convenient to compare SC2 with SC1, as the former scenario only differs from the latter by the values of the river's discharge. Therefore, in determining ΔV = (V(SCI)-V(SCJ)), SC1 and SC2 correspond, respectively, to SCI and SCJ.

Considering the salinity time series (Figure 3), the values observed for SC2 are nearly constant for most stations and close to the ocean values, 34 PSU. Under this scenario, the lagoon is, therefore, mostly filled with ocean waters, and no evidence of the influence of the river is found, even near the RIFEN areas, as observed in the snapshots of Figure 5. Indeed, Δ(Salinity) time series (Figure 4) show that the RIFEN stations present values as low as −30 PSU (namely for St3 and 4), during the spring tide, corresponding to an extreme salinity change between SC1 (~5 PSU) and SC2 (~34 PSU) (see Table 4). On the other hand, St1, St2, and St5 show Δ(Salinity) ~0, reflecting the strong influence of the ocean flow for the two scenarios. Overall, SC2, depicts a consistent salinity intrusion up to the lagoon RIFEN areas, as can be observed in the snapshots of the surface salinity (Figure 5), reflecting not only the increase of the ocean inflow to the lagoon, but also the reduction of the freshwater discharge from the rivers.

The water temperature time series of Figure 6, show that the values for SC2m are in the range of 18-20 °C, and are well below those for SC1, for all the stations. On the other hand, St1 shows lower water temperature values (18.0–19.0 °C), while the remaining stations, namely St2 and RIFEN, present slightly higher ones (18.5–20 °C). Δ(Temperature) time series (Figure 7) show positive maximum and average values, ranging within 0.5–2.0 °C, as can be observed in Table 5, confirming the overall decreasing in the water temperature for SC2 relatively to SC1. This result reflects the dominant influence of the ocean and is in line with what was previously observed for the salinity. Indeed, the river discharges reduction, together with the increasing of the ocean cold water inflow into the lagoon, leads to an overall water temperature decrease. Figure 8 presents snapshots of the surface temperature for the scenarios. It clearly depicts the intrusion of the ocean cold water (in blue) into the lagoon, while the front between the warm water (in red) and the lagoon mix-water is situated far ahead.

The time series of the inorganic nitrogen concentration, IN, for SC2, (Figure 9) show that the concentration values range between 0.2 and 1.0 mg L^{-1}, which are significantly lower than those for SC1 (0.5–2 mg L^{-1}). Furthermore, they show no significant evidence of the spring-neap tide modulation. The time series of the inorganic nitrogen concentration difference between SC2 and SC1, Δ(IN), (Figure 10), show positive values, while the RIFEN stations reach maximum values as high as 1.5 mg L^{-1} (Table 6), reflecting the concentration increase for SC1 during the spring tide period. The scenario reflects, therefore, the conjunction of two situations: the increase of the ocean flow (poor in IN) and the reduction of the rivers flow (rich in IN), leading to an overall decrease of IN concentration in the lagoon, as observed in Figure 11, which corresponds to snapshots of the inorganic nitrogen concentration, IN, for the scenarios.

The time series of the Secchi depth, ScD, for SC2, (Figure 12), show small amplitude oscillations, with values varying within a tight range (~1.2 m–1.8 m), while the snapshots of Figure 14 evidence high values for most of the lagoon areas (~1.8 m). Except for the spring-neap tide period, SC2 shows similar values as SC1, even though slightly lower, as the scenario presents no spring-neap tide modulation, contrarily to SC2. During the spring-neap tide period, the ScD for SC1 values fall below those of SC2, reflecting the significant amplitude oscillation of SC1, namely at the RIFEN stations. The time series of the Secchi depth difference between SC2 and SC1, Δ(ScD), (Figure 13), show, in general, negative values, but a closer look at the figure evidences that δ(ScD) experiences significant fluctuations, showing alternation between positive and negative values, as can be observed for the main river station, St4 (−1 m; 0.5 m), (Table 7). It is worth noting that St5 shows a singular behavior during the spring tide period, corresponding to positive values of Δ(ScD) (up to 0.2 m) and, therefore, a significant decrease of ScD for the scenario. Under the scenario, the water column shows mix-water behavior during the spring tide: the deeper water stations, under the ocean water influence, St1 and St2, seem not significantly affected by the scenario |Δ(ScD)| < 0.1 m, while the RIFEN stations show ScD increased,

with significant fluctuations. This result evidences a spatial distribution of the ScD, under the influence of the ocean and the river waters.

Just like Secchi depth, ScD, the time-series of the carbon phytoplankton concentration, PC, for SC2, (Figure 15), do not evidence significant spring-neap tide modulation and present slightly higher values than SC1 (<0.2 mg L^{-1}), except for the spring-neap tide period, when the last presents phytoplankton blooms, as previously observed. Indeed, during this period, the RIFEN stations present positive values of the carbon phytoplankton concentration difference, Δ(PC), (Figure 16), reaching maximum values as high as 0.5 mg L^{-1} (Table 8), while |Δ(PC)| is small (<0.1 mg L^{-1}), except for the spring-neap tide period. It is worth noting that St1, St2, and St5 do not show significant Δ(PC) oscillation values (<0.1 mg L^{-1}). Furthermore, the snapshots of Figure 17(1c, 2c) show a surprising phytoplankton bloom along the Ílhavo channel, as well as a localised spot along the S. Jacinto channel, between St5 and St8. As the river discharges for SC2 (dry scenario) were significantly lowered, smaller values were expected for PC for the scenario relatively to SC1, since the discharge of nutrients decreased with the flow. Nevertheless, the boundary conditions for the physical and the biogeochemical variables remained unchanged for the scenario. However, the phytoplankton growth depends not only on light and nutrients availability but also on the turbulence state of the flow, which in this scenario may play a key role. Indeed, the turbulent eddy diffusivity coefficients (not shown), calculated with the help of the k-ε model showed significant increase for SC2 relatively to SC1, the maximum values were almost 50% higher for St3, St4, and St5 (from the reference value of 1.5 m/s^2, 3.5 m/s^2 m/s^2 and 2.5 m/s^2, respectively) and 100% for St5 (from the reference value of 0.8 m/s2). Therefore, even in a dry situation, nutrients located at the river boundaries can be brought into the tidal flow, during ebbing, and dispersed by the turbulence (eddy dispersion), thus becoming available to the phytoplankton. This result will be discussed in the next section.

4.3. The Warm Climate Scenario (SC3)

This scenario deals with a warm climate at the lagoon coastal area, corresponding to an increase of the air temperature of 2 °C, relatively to the baseline, considering an SLR situation, as presented in Table 3. Figures 6 and 7 present water temperature and Δ(Temperature) time series. Comparing SC3 to SC1, Δ(Temperature) presents smaller amplitude oscillation (~−0.5 °C), with the water temperature ranging between 18.5 and 22 °C. St2 and St3 show the highest value (~22 °C), while St1 the lowest one (~18.5 °C). The salinity and the biogeochemical variables are not presented, as the results did not evidence any significant changes between SC1 and SC3.

4.4. The Taylor Diagram for the Scenarios

Figures 18–21 present Taylor diagrams for salinity, temperature, IN and PC, respectively and for the scenarios SC1 and SC2. The diagrams graphically compare BS, SC1 (M1 in the diagram) and SC2 (M2 in the diagram), using centered root-mean-square deviation, RMSD, between two simulations. Only six stations out of eight, are presented, as the analysis does not affect the generality of the results. This method enables the impact of changes induced by the scenarios on each variable and station to be graphically assessed. Furthermore, with the help of the RMSD contours (in green in the figures), it allows the changes to be statistically quantified. Furthermore, it is possible to read in the diagram the standard deviation of each scenario (on the axes), as well as the correlation between them (values in blue). Moreover, by measuring the distance between the RMSD contours, the difference between two simulations can be assessed. In general, the results are in line with those of the previous sections. Indeed, high values of RMSD for salinity can be observed, which are of the order of 6–7 PSU, for the rivers stations St3 and St4, while the remaining stations (St2, St5, St6, and St8) show moderate values, of the order of 1–3 PSU. Likewise, temperature presents RMSD values in the range of 0.2–0.6 °C, while IN and PC show values of the order of 0.2–04 mg L^{-1} and 0.1–0.2 mg L^{-1}, respectively.
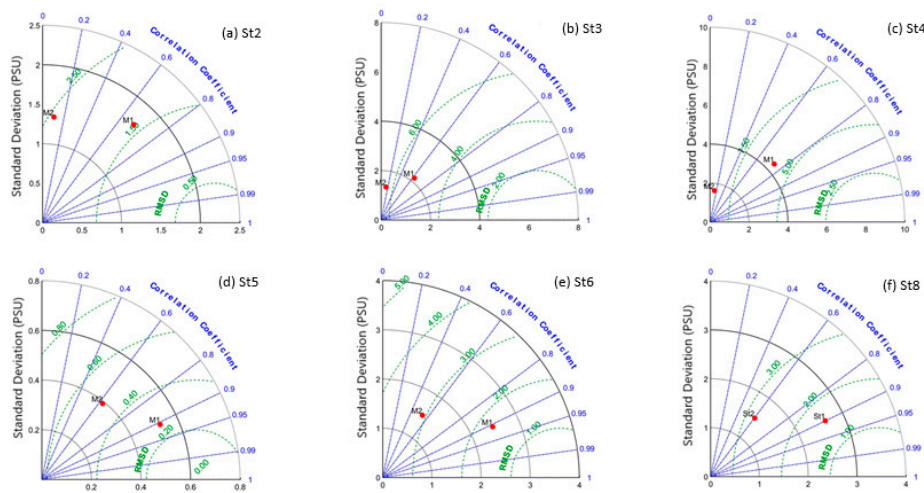
Figure 18. Taylor diagrams for SC1 (M1) and SC2 (M2), for salinity and the lagoon stations: (**a**) St1, (**b**) St3, (**c**) St4, (**d**) St5, (**e**) St6 and (**f**) St8.
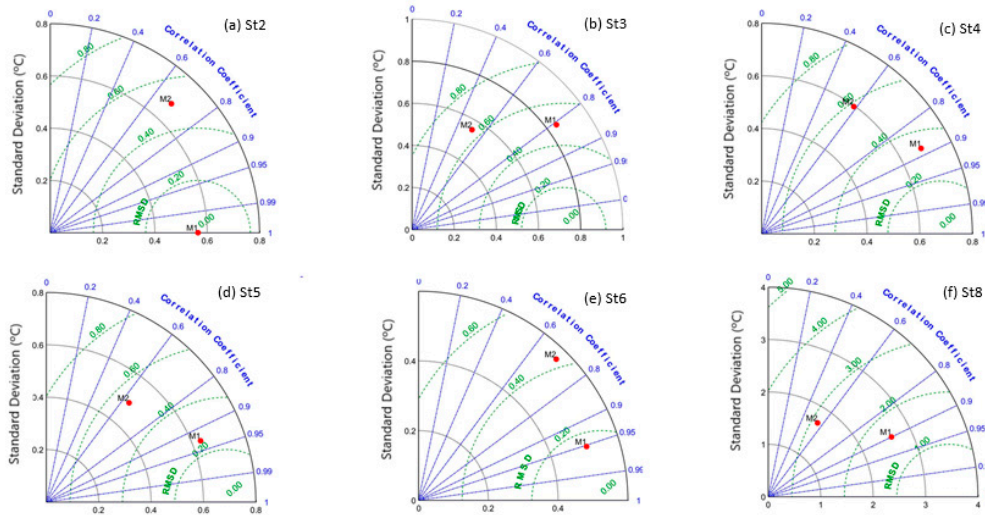

Figure 19. Taylor diagrams for SC1 (M1) and SC2 (M2), for temperature and the lagoon stations: (**a**) St1, (**b**) St3, (**c**) St4, (**d**) St5, (**e**) St6 and (**f**) St8.
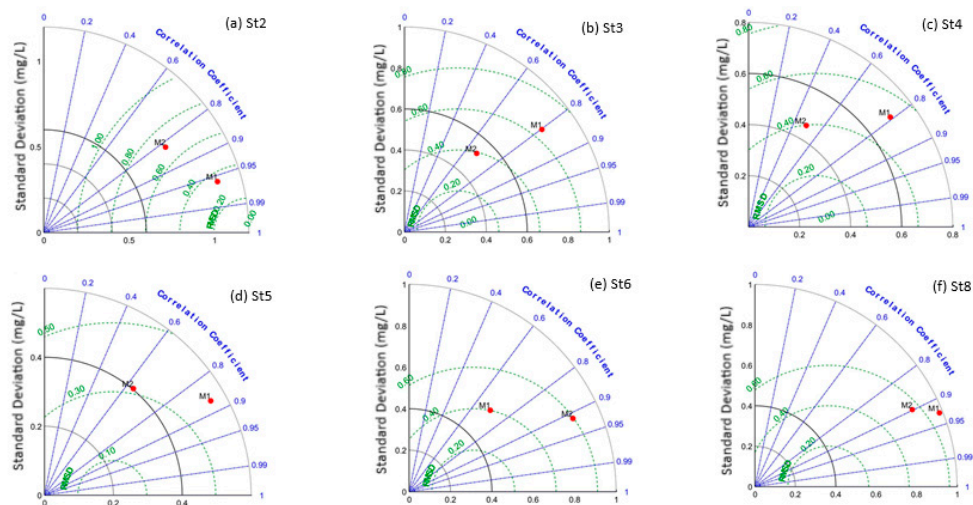

Figure 20. Taylor diagrams for SC1 (M1) and SC2 (M2), for inorganic nitrogen concentration, IN, and the stations: (**a**) St1, (**b**) St3, (**c**) St4, (**d**) St5, (**e**) St6 and (**f**) St8.
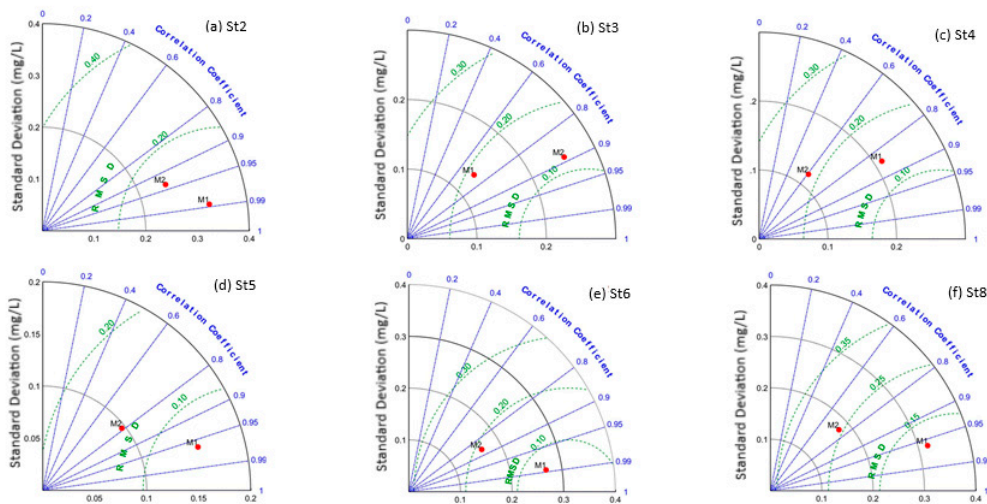
Figure 21. Taylor diagrams for SC1 (M1) and SC2 (M2), for carbon phytoplankton, PC, and the lagoon stations: (**a**) St1, (**b**) St3, (**c**) St4, (**d**) St5, (**e**) St6 and (**f**) St8.

5. Discussion

This study aims to assess the Ria de Aveiro physical and biogeochemical status, under future climate scenarios, considering the impact of climate changes in the lagoon coastal area, namely the rise of the sea level and of the amplitude of the M_2 component of the tide, the changes of the river discharges, and the rising of the air temperature. It used a coupled physical and eutrophication model that simulates the main state variables of the water column.

The baseline scenario (BS) showed that the salinity patterns of the lagoon are mainly influenced by the exchange with the ocean waters. Even under mean rivers discharge the salinity distributions for the late summer evidenced that the ocean water influence reaches the lagoon upper areas, where high values of salinity (~34 PSU) are observed, as well as important gradients of salinity (0–34 PSU). Indeed, the stations St3, St4, St6, St7, and St8 presented wide ranges of salinity amplitude oscillations (5–34 PSU or 15–34 PSU) during the spring-neap tide period, evidencing the competing influence of rivers and ocean waters. St2, situated close to the ocean boundary, at the mouth of the Espinheiro channel connecting the major river (Vouga) to the ocean, is, actually, evidence of the conjugation of the river and the ocean waters. The salinity values are typical for mix-waters, varying within the range of 20–34 PSU, similar to those observed by Vaz et al. [45]. As the tide evolves during the flooding period, the ocean waters flow inside the lagoon and are pushed toward the RIFEN areas, increasing their salinity, while during the ebbing period freshwaters disperse into the lagoon central areas and, occasionally, reach the lagoon mouth, mainly through the Espinheiro channel. Nevertheless, the result points out that, only during the neap tide, the influences between the river and the ocean water are balanced. Otherwise, there is a net ocean dominance. Concerning the water temperature, the results evidenced variations within the range of 18.0–20 °C for most of the lagoon stations, and for the late summer, revealing a 2 °C amplitude oscillation (intraday, fortnight, and spatial modulations), and reflecting a competition between cold and warm water from the ocean and the rivers, respectively, as well as the diurnal heating of the water column, generating a net horizontal water temperature gradient.

Under the future climate scenarios, i.e., the combined effect of mean SLR and M_2 tidal amplitude rise, the results show a significant impact on the salinity patterns. The salinity values are considerably higher when comparing to BS. Indeed, under the scenarios SC1 (the mean sea level, MSLR, scenario) and SC2 (MSLR and dry summer situation scenario), there is an increase of the ocean inflow into the lagoon. The water reaches the lagoon central and the major rivers and far end areas (RIFEN areas), leading to an overall increase of salinity. Stations St1, St2, and St5 do not evidence, under SC1, any significant influence of the river waters, as the salinity was almost constant (~34 PSU), while St3, St4, St6, St7, and St8, under the influence of the freshwaters, showed a high salinity range (20–34 PSU),

namely during the spring tides. Under the scenario SC2, corresponding to the combined effect of MSLR, M2R, and low river discharge, it was found that the salinity becomes almost constant (~34 PSU) for the lagoon, reflecting its infilling with ocean water, a situation resulting from the combined effect of increasing ocean flow and decreasing of the river's freshwater discharge. Therefore, SC2 generates a net increase of the landward propagation of oceanic waters, while the freshwater influence is restricted to the RIFEN areas, which become exposed to saltier waters.

Concerning the water temperature, under both SC1 and SC2, when comparing to BS, the results depict a consistent water temperature decrease, of the order of 0.5–2.0 °C, at areas close to the lagoon mouth, while the central and far end areas show moderate reduction (~1.0 °C). Furthermore, SC2 shows lower water temperature values than SC1 for all stations. This situation, which is in line with the salinity result, demonstrated that under SLR, a net increase of the ocean flow (cold and salty water) into the lagoon is generated. Concerning the warm climate scenario, SC3, the results show an overall water temperature increase (~0.5 °C) relatively to SC1, for a range of water temperature of 19–22 °C.

The biogeochemical variables reflect, in general, the dynamics of the lagoon depicted by the salinity and the water temperature results. The discussion will be confined to SC1 and SC2 scenarios, as SC3 did not show any significant impact on the biogeochemical variables. The results point out to an overall decrease of the IN concentrations, under SC1 and SC2. Indeed, significant values of $|\Delta(IN)|$ within the range 1–1.5 mg L^{-1} were observed, for SC1, for the RIFEN areas. Again, the results demonstrated that an increase of the ocean flow (cold and salty water) or the reduction of the river flow, under climate changes, ultimately lead to an overall decrease of the inorganic nitrogen concentration. Likewise, the Secchi depth, ScD, evidenced the competing influence between the rivers and the ocean waters, namely during the spring tide period. The increase of the ocean flow brings transparent water into the lagoon, while the rivers do the opposite. Indeed, SC1 shows an overall increase of ScD relatively to BS (corresponding to negatives values of the Secchi depth difference, $\Delta(ScD)$, between SC1 and BS of the order of -1 m near the water of the river during the spring tide period, which corresponds to an overall increase of the water transparency of the lagoon. SC2 evidenced a mixed behavior, even though, excluding the spring tide period, $\Delta(ScD)$ tend to be positive and small (~0.1 m), still reflecting an increase of ScD. Nevertheless, as the river discharge was small, a more consistent increase of the ScD was expected. The carbon phytoplankton concentration, PC, responds to SC1 as expected: the significant concentration reduction relatively to BS reflects the overall reduction of the IN concentration observed for the scenario. Nevertheless, concerning SC2, when compared to SC1, the time series did not present, besides the typical diurnal and the semi-diurnal variability, any significant spring-neap tide modulation, as was observed for BS and SC1. Except for this period, PC concentrations for SC2 showed unexpected slightly higher values than those for SC1. Indeed, as the river discharge was small, the opposite behavior was expected. Furthermore, it can be observed from the PC snapshots for SC2 (Figure 17(1c,2c)), that the 'phytoplankton blooms' which were located at the RIFEN areas are no longer present, while new ones reappear at the S. Jacinto channel and the southern areas, along the Ílhavo channel. Therefore, a scenario of river flow reduction should affect the phytoplankton distribution and the location of the bloom. Indeed, it should be considered that the phytoplankton growth depends not only on the light and nutrients availability but also on the turbulence transport, which is the essential mechanism for dispersion in natural water. Changes in the turbulent state of the flow (that is the eddy diffusivity), while the nutrient conditions at the river boundaries are unchanged, may be accounted for by the major changes in the phytoplankton concentration, as well as the location of the bloom spots in SC2. Nutrients may be made more effectively available to phytoplankton through this mechanism. During the ebb, tidal flow carries nutrients from the rivers to the central area of the lagoon, where they are dispersed by turbulence. A warmer climate scenario, SC3, seems not to affect the main biogeochemical state variable. Nevertheless, it is well known that the biogeochemical status of the water column can be affected by oxygen concentration and saturation, which are temperature-dependent. On the other hand, the oxygen concentration may, in turn, influence nutrient cycling. The study was not focused on this issue, but the results suggest no

significant relationship between these variables, at least under the frame of the current model. Finally, it was demonstrated that the Taylor diagram may be a valuable to assess, graphically and statistically, the impact of the scenarios. From a simple analysis of the diagrams, the major results were highlighted. Indeed, the diagrams give similar results to those previously obtained, namely, high values of RMSD for the salinity (~6–7 PSU), for the rivers stations St3 and St4 but moderate values (~1–3 PSU) for the remaining stations (St2, St5, St6, and St8). The RMSD values for water temperature, IN and PC, are, respectively, within the ranges of 0.2–0.6, 0.2–0.4 mg L^{-1}, and 0.1–0.2 mg L^{-1}, which are of the same order as Δ(Temperature), Δ(IN) and Δ(PC), previously obtained.

From the results, it can be concluded that SLR will impact not only the physical but also the biogeochemical status of the water column, as well as their interplay. The impacting of global warming on the physical properties of the water system ultimately affects its biogeochemistry, namely the phytoplankton abundance and distribution.

Future model applications should include the influence of the sediment dynamics in the turbidity evolution of the water column, the contribution of the biogeochemical processes in the upper layer of the sediment bed (diagenesis), and the influence of the *N/P* ratio in the nutrient and the phytoplankton concentration dynamics. The role of the temperature and dissolved oxygen in the biogeochemistry of the water column should also be addressed. A study encompassing all these issues in the frame of a changing climate is a true challenge.

6. Concluding Remarks

The present work was designed to assess the impact of climate changes on the physical and biogeochemical status of the Ria de Aveiro lagoon, through the analysis of the combined effects of: the rising of the mean sea level and of the amplitude of the M$_2$ tidal constituent, the decreasing of the river discharges and the increasing average air temperature.

Under the present climate and considering a late summer situation and mean river discharges, the salinity distribution patterns attest the ocean water dominance on the lagoon. On the other hand, the competing influence between the ocean and the water of the major river is limited to the lagoon upper reaches during the spring tide period. Except for this period, high values of salinity (20–34 PSU) were observed even at the lagoon far ends. The water temperature also reflected the ocean dominance, even though the competing influence of the cold water from the ocean and warm water from the lagoon upper reaches is more complex and affected by the diurnal heating of the water column. Under MSLR and M2R scenarios, the results point to an overall increase of the ocean water transport (cold and salty water) into the lagoon, resulting in a consistent increase of the salinity up to the RIFEN areas, where high values are observed (20–34 PSU), as well as the decrease of water temperature in the lagoon (0.5–1.5 °C). The biogeochemical variables under the same scenarios reflected the increase of the oceanic flow (transparent and inorganic nitrogen-poor water) or the reduction of the river flow (inorganic nitrogen-rich water) into the lagoon. An overall decreasing of the inorganic nitrogen concentration for all the lagoon stations is evident, while the carbon phytoplankton responded with significant concentration reduction. Under the combined effect of MSLR, M2R, and dry summer, corresponding to very low river discharges, the results demonstrate an overall increase of the salinity and a decrease of the water temperature of the lagoon. The main lagoon areas will present high salinity values, ~34 PSU, reflecting a net increase of ocean water inflow. In this situation, the upper heads of the main channels and the river mouths show characteristics of brackish waters. The salinity intrusion is, therefore, an important outcome of the scenarios simulated for the lagoon, which is a serious issue for the riverine and the salt marsh areas. The water temperature experienced a decrease in the range of 0.5–2.0 °C. Concerning the nutrients, the results point out to a net decrease of the inorganic nitrogen concentration inside the lagoon, reflecting the increase of the low concentrated water flow from the ocean. The carbon phytoplankton concentration has decreased reflecting, as expected, the trend in nutrients. Nevertheless, the unexpected increase in phytoplankton concentration or blooms observed at some lagoon area in a

situation of small river discharges can be explained by the turbulent dispersion, which plays a key role in the nutrient dispersion and redistribution, contributing for the phytoplankton growth.

Nomenclature

SLR	sea level rise
MSLR	mean sea level rise
M2R	M2 tidal constituent rise
IN	Inorganic Nitrogen
BS	baseline simulation
SC1, SC2, SC3	scenario simulations
RIFEN	Major rivers and the lagoon far end areas

References

1. IPCC. 2018: Summary for Policymakers. In *Global Warming of 1.5 °C. An IPCC Special Report on the Impacts of Global Warming of 1.5 °C above Pre-Industrial Levels and Related Global Greenhouse Gas Emission Pathways, in the Context of Strengthening the Global Response to the Threat of Climate Change, Sustainable Development, and Efforts to Eradicate Poverty*; Masson-Delmotte, V., Zhai, P., Pörtner, H.O., Roberts, D., Skea, J., Shukla, P.R., Pirani, A., Moufouma-Okia, W., Péan, C., Pidcock, R., et al., Eds.; World Meteorological Organization: Geneva, Switzerland, 2018; p. 32.

2. Smith, T.M.; Reynolds, R.W.; Peterson, T.C.; Lawrimore, J. Improvements to NOAA's historical merged land-ocean surface temperature analysis (1880–2006). *J. Clim.* **2008**, *21*, 2283–2296. [CrossRef]

3. Keenlyside, N.S.; Latif, M.; Jungclaus, J.; Kornblueh, L.; Roeckner, E. Advancing decadal-scale climate prediction in the North Atlantic Sector. *Nature* **2008**, *453*, 84–88. [CrossRef] [PubMed]

4. Hartmann, D.L.; Klein Tank, A.M.G.; Rusticucci, M.; Alexander, L.V.; Brönnimann, S.; Charabi, Y.; Dentener, F.J.; Dlugokencky, E.J.; Easterling, D.R.; Kaplan, A.; et al. Observations: Atmosphere and Surface. In *Climate Change 2013: The Physical Science Basis. Contribution of Working Group I to the Fifth Assessment Report of the Intergovernmental Panel on Climate Change*; Stocker, T.F., Qin, D., Plattner, G.-K., Tignor, M., Allen, S.K., Boschung, J., Nauels, A., Xia, Y., Bex, V., Midgley, P.M., Eds.; Cambridge University Press: Cambridge, UK; New York, NY, USA, 2013; pp. 159–254.

5. Collins, M.; Knutti, R.; Arblaster, J.; Dufresne, J.-L.; Fichefet, T.; Friedlingstein, P.; Gao, X.; Gutowski, W.J.; Johns, T.; Krinner, G.; et al. Long-term Climate Change: Projections, Commitments and Irreversibility. In *Climate Change 2013: The Physical Science Basis. Contribution of Working Group I to the Fifth Assessment Report of the Intergovernmental Panel on Climate Change*; Stocker, T.F., Qin, D., Plattner, G.-K., Tignor, M., Allen, S.K., Boschung, J., Nauels, A., Xia, Y., Bex, V., Midgley, P.M., Eds.; Cambridge University Press: Cambridge, UK; New York, NY, USA, 2013; pp. 1029–1136.

6. Rhein, M.A.; Rintoul, S.R.; Aoki, S.; Campos, E.; Chambers, D.; Feely, R.A.; Gulev, S.; Johnson, G.C.; Josey, S.A.; Kostianoy, A.; et al. Observations: Ocean. In *Climate Change: The Physical Science Basis. Contribution of Working Group I to the Fifth Assessment Report of the Intergovernmental Panel on Climate Change*; Stocker, T.F., Qin, D., Plattner, G.-K., Tignor, M., Allen, S.K., Boschung, J., Nauels, A., Xia, Y., Bex, V., Midgley, P.M., Eds.; Cambridge University Press: Cambridge, UK; New York, NY, USA, 2013; pp. 255–315.

7. Kumbier, K.; Carvalho, R.C.; Woodroffe, C.D. Modelling Hydrodynamic Impacts of Sea-Level Rise on Wave-Dominated Australian Estuaries with Differing Geomorphology. *J. Mar. Sci. Eng.* **2018**, *6*, 66. [CrossRef]

8. Huber, D.G.; Gulledge, J. *Extreme Weather and Climate Change: Understanding the Link and Managing the Risk. Science and Impacts Program*; Center for Climate and Energy Solutions: Arlington, VA, USA, 2011. Available online: http://www.c2es.org/publications/extreme-weather-and-climate-change (accessed on 1 October 2019).

9. Ummenhofer, C.C.; Meehl, G.A. Extreme weather and climate events with ecological relevance: A review. *Philos. Trans. R. Soc. B* **2017**, *372*, 20160135. [CrossRef] [PubMed]

10. Church, J.A.; Clark, P.U.; Cazenave, A.; Gregory, J.M.; Jevrejeva, S.; Levermann, A.; Merrifield, M.A.; Milne, G.A.; Nerem, R.S.; Nunn, P.D.; et al. Sea Level Change. In *Climate Change 2013: The Physical Science Basis. Contribution of Working Group I to the Fifth Assessment Report of the Intergovernmental Panel on Climate Change*; Stocker, T.F., Qin, D., Plattner, G.-K., Tignor, M., Allen, S.K., Boschung, J., Nauels, A., Xia, Y., Bex, V., Midgley, P.M., Eds.; Cambridge University Press: Cambridge, UK; New York, NY, USA, 2013; pp. 1137–1216.

11. Carrasco, A.R.; Ferreira, O.; Roelvink, D. Coastal lagoons and rising sea level: A review. *Earth Sci. Rev.* **2016**, *154*, 356–368. [CrossRef]

12. Rahmstorf, S. A semi-empirical approach to projecting future sea-level rise. *Science* **2007**, *315*, 368–370. [CrossRef]

13. Vaughan, D.G.; Comiso, J.C.; Allison, I.; Carrasco, J.; Kaser, G.; Kwok, R.; Mote, P.; Murray, T.; Paul, F.; Ren, J.; et al. Observations: Cryosphere. In *Climate Change 2013: The Physical Science Basis. Contribution of Working Group I to the Fifth Assessment Report of the Intergovernmental Panel on Climate Change*; Stocker, T.F., Qin, D., Plattner, G.-K., Tignor, M., Allen, S.K., Boschung, J., Nauels, A., Xia, Y., Bex, V., Midgley, P.M., Eds.; Cambridge University Press: Cambridge, UK; New York, NY, USA, 2013; pp. 317–382.

14. Le Bars, D. Uncertainty in sea level rise projections due to the dependence between contributors. *Earths Future* **2018**, *6*, 1275–1291. [CrossRef]

15. Nauels, A.; Malte Meinshausen, M.; Mengel, M.; Lorbacher, K.; Wigley, T.M.L. Synthesizing Long-Term Sea Level Rise Projections—The MAGICC Sea Level Model. Geoscientific Model Development Discussions. *Geosci. Model. Dev.* **2017**, *10*, 2495–2524. [CrossRef]

16. Antunes, C.; Taborda, R. Sea level at Cascais Tide Gauge: Data, Analysis and Results. *J. Coast. Res.* **2009**, *56*, 218–222.

17. Lopes, C.L.; Silva, P.A.; Dias, J.M.; Rocha, A.; Picado, A.; Plecha, S.; Fortunato, A.B. Local sea level change scenarios for the end of the 21st century and potential physical impacts in the lower Ria de Aveiro (Portugal). *Cont. Shelf Res.* **2011**, *31*, 1515–1526. [CrossRef]

18. Pelling, H.E.; Green, J.A.M. Sea level rise and tidal power plants in the Gulf of Maine. *J. Geophys. Res. Oceans* **2013**, *118*, 2863–2873. [CrossRef]

19. Pelling, H.E.; Green, J.A.M.; Ward, S.L. Modelling tides and sea-level rise: To flood or not to flood. *Ocean Model.* **2013**, *63*, 21–29. [CrossRef]

20. Pickering, M.; Horsburgh, K.J.; Blundell, J.R.; Hirschi, J.J.M.; Nicholls, R.J.; Verlaan, M.; Wells, N.C. The impact of future sea-level rise on the global tides. *Cont. Shelf Res.* **2017**, *142*, 50–68. [CrossRef]

21. Idier, D.; Paris, F.; Le Cozannet, G.; Boulahya, F.; Dumas, F. Sea-level rise impacts on the tides of the European Shelf. *Cont. Shelf Res.* **2017**, *137*, 56–71. [CrossRef]

22. Anthony, A.; Atwood, J.; August, P.; Byron, C.; Cobb, S.; Foster, C.; Fry, C.; Gold, A.; Hagos, K.; Heffner, L.; et al. Coastal lagoons and climate change: Ecological and social ramifications in U.S. Atlantic and Gulf coast ecosystems. *Ecol. Soc.* **2009**, *14*, 1–8. [CrossRef]

23. Hayes, M.O. Barrier islands. In *Encyclopedia of Coastal Science*; Schwartz, M.L., Ed.; Springer: Dordrecht, The Netherlands, 2005; pp. 117–119.

24. Zhang, K.; Douglas, B.C.; Leatherman, S.P. Global warming and coastal erosion. *Clim. Chang.* **2004**, *64*, 41–58. [CrossRef]

25. Bird, E.C.F. Physical setting and geomorphology of coastal lagoons. In *Coastal Lagoon Processes*; Kjerfve, B., Ed.; Elsevier: Amsterdam, The Netherlands, 1994; Volume 2, pp. 9–40.

26. Zimmerman, J.T.F. The flushing of well-mixed tidal lagoons and its seasonal fluctuation. In *Coastal Lagoon Research, Present and Future*; UNESCO Technical Papers in Marine Science; UNESCO: Paris, France, 1981; Volume 3, pp. 15–26.

27. Lloret, J.; Marín, A.; Marín-Guirao, L. Is coastal lagoon eutrophication likely to be aggravated by global climate change? *Estuar. Coast. Shelf Sci.* **2008**, *78*, 403–412. [CrossRef]

28. Turner, R.E. *Coastal Ecosystems of the Gulf of Mexico and Climate Change. Integrated Assessment of the Climate Change Impacts on the Gulf Coast Region*; Ning, Z.H., Turner, R.E., Doyle, T., Abdollahi, K.K., Eds.; Gulf Coast Climate Change Assessment Council and Louisiana State University Graphic Services: Washington, DC, USA, 2003; pp. 85–103.

29. Bopp, L.; Le Quéré, C.; Heimann, M.; Manning, A.C.; Monfray, P. Climate-induced oceanic oxygen fluxes: Implications for the contemporary carbon budget. *Glob. Biogeochem. Cycles* **2002**, *16*, 1022. [CrossRef]

30. Joos, F.; Plattner, G.K.; Stocker, T.F.; Körtzinger, A.; Wallace, D.W.R. Trends in marine dissolved oxygen: Implications for ocean circulation changes and the carbon budget. *Eos Trans. Am. Geophys. Union* **2003**, *84*, 197–207. [CrossRef]

31. D'Avanzo, C.; Kremer, J.N. Diel oxygen dynamics and anoxic events in a eutrophic estuary of Waquoit Bay, Massachusetts. *Estuaries* **1994**, *17*, 131–139. [CrossRef]

32. Mackenzie, B.R.; Gislason, H.; Möllmann, C.; Köster, F.W. Impact of 21st century climate change on the Baltic Sea fish community and fisheries. *Glob. Chang. Biol.* **2007**, *13*, 1348–1367. [CrossRef]

33. Conley, D.J.; Carstensen, J.; Aertebjerg, G.; Christensen, P.B.; Dalsgaard, T.; Josefson, J.L.S.; Josefson, A.B. Long-term changes and impacts of hypoxia in Danish coastal waters. *Ecol. Appl.* **2007**, *17*, S165–S184. [CrossRef]

34. Tomanek, L.; Somero, G.N. Evolutionary and acclimation-induced variation in the heat-shock responses of congeneric marine snails (genus Tegula) from different thermal habitats: Implications for limits of thermotolerance and biogeography. *J. Exp. Biol.* **1999**, *202*, 2925–2936. [PubMed]

35. Oviatt, C.A. The changing ecology of temperate coastal waters during a warming trend. *Estuaries* **2004**, *27*, 895–904. [CrossRef]

36. Blintz, J.C.; Nixon, S.; Buckley, B.; Granger, S. Impacts of temperature and nutrients on coastal lagoon plant communities. *Estuaries* **2003**, *26*, 765–776. [CrossRef]

37. Paerl, H.; Valerie, P. Climate change: Links to global expansion of harmful cyanobacteria. *Water Res.* **2019**, *46*, 1349–1363. [CrossRef]

38. Mike3. Hydrodynamic and Transport Module. A Scientific Description, DHI Water and Environment. Denmark. 2017. Available online: https://www.mikepoweredbydhi.com/download/mike-2019 (accessed on 1 October 2019).

39. Mike3. Eutrophication Model. A Scientific Description, ECO Lab-A Numerical Laboratory for Ecological Modelling, DHI Water and Environment. Denmark. 2017. Available online: https://www.mikepoweredbydhi.com/download/mike-2019 (accessed on 1 October 2019).

40. Lopes, C.L.; Dias, J.M. Tidal dynamics in a changing lagoon: Flooding or not flooding the marginal regions. *Estuar. Coast. Shelf Sci.* **2015**, *167*, 14–24. [CrossRef]

41. Lopes, C.L.; Dias, J.M. Assessment of flood hazard during extreme sea levels in a tidally dominated lagoon. *Nat. Hazards* **2015**, *77*, 1345–1364. [CrossRef]

42. Lopes, C.L.; Azevedo, A.; Dias, J.M. Flooding assessment under sea level rise scenarios: Ria de Aveiro case study. *J. Coast. Res.* **2013**, *65*, 766–771. [CrossRef]

43. Lopes, C.L.; Alves, F.L.; Dias, J.M. Flood risk assessment in a coastal lagoon under present and future scenarios: Ria de Aveiro case study. *Nat. Hazards* **2017**, *89*, 1307–1325. [CrossRef]

44. Vargas, C.I.C.; Vaz, N.; Dias, J.M. An evaluation of climate change effects in estuarine salinity patterns: Application to Ria de Aveiro shallow water system. *Estuar. Coast. Shelf Sci.* **2017**, *189*, 33–45. [CrossRef]

45. Dias, J.M. Contribution to the Study of the Ria de Aveiro Hydrodynamics. Ph.D. Thesis, Universidade de Aveiro, Aveiro, Portugal, 2001; p. 288.

46. Vaz, N.; Dias, J.M. Hydrographic characterization of an estuarine tidal channel. *J. Mar. Syst.* **2008**, *70*, 168–181. [CrossRef]

47. Dias, J.M.; Lopes, J.F.; Dekeyser, I. Hydrological characterisation of Ria de Aveiro lagoon, Portugal, in early summer. *Oceanol. Acta* **1999**, *22*, 473–485. [CrossRef]

48. Dias, J.M.; Lopes, J.F.; Dekeyser, I. Lagrangian transport of particles in Ria de Aveiro lagoon, Portugal. *Phys. Chem. Earth B* **2001**, *26*, 729–734. [CrossRef]

49. Dias, J.M.; Lopes, J.F.; Dekeyser, I. A numerical system to study the transport properties in the Ria de Aveiro lagoon. *Ocean Dyn.* **2003**, *53*, 220–231. [CrossRef]

50. Dias, J.M.; Lopes, J.F. Implementation and evaluation of hydrodynamic, salt and heat transport models: The case of Ria de Aveiro Lagoon, Portugal. *Environ. Model. Softw.* **2006**, *21*, 1–15. [CrossRef]

51. Fortunato, A.B.; Rodrigues, M.; Dias, J.M.; Lopes, C.; Oliveira, A. Generating inundation maps for a coastal lagoon: A case study in the Ria de Aveiro (Portugal). *Ocean Eng.* **2013**, *64*, 60–71. [CrossRef]

52. Vaz, L.; Plecha, S.; Dias, J.M. Coastal wave regime influence on Ria de Aveiro inlet dynamics. *J. Coast. Res.* **2013**, *65*, 1605–1610. [CrossRef]

53. Vicente, C.M. *Caracterização Hidráulica e Aluvionar da Ria de Aveiro, Utilização de Modelos Hidráulicos no Estudo de Problemas da Ria*; Utilização 1719 de modelos hidráulicos no estudo de problemas; Câmara Municipal de Aveiro: Aveiro, Portugal; Jormadas da Ria de Aveiro, Ed.; 1985; Volume III, pp. 41–58.

54. Génio, L.; Sousa, A.; Vaz, N.; Dias, J.M.; Barroso, C. Effect of low salinity on the survival of recently hatched veliger of *Nassarius reticulatus* (L.) in estuarine habitats: A case study of Ria de Aveiro. *J. Sea Res.* **2008**, *59*, 133–143. [CrossRef]

55. Moreira, M.H.; Queiroga, H.; Machado, M.M.; Cunha, M.R. Environmental gradients in a southern estuarine system: Ria de Aveiro, Portugal, implication for soft bottom macrofauna colonization. *Aquatic Ecol.* **1993**, *27*, 465–482. [CrossRef]

56. Almeida, M.A.; Cunha, M.A.; Alcântara, F. Relationship of bacterioplankton production with primary production and respiration in a shallow estuarine system, Ria de Aveiro, NW Portugal. *Microbiol. Res.* **2005**, *160*, 315–328. [CrossRef] [PubMed]

57. Rodrigues, M.; Oliveira, A.; Queiroga, H.; Fortunato, A.B.; Zhang, Y.J. Three-dimensional modelling of the lower trophic levels in the Ria de Aveiro (Portugal). *Ecol. Model.* **2009**, *220*, 1274–1290. [CrossRef]

58. Lopes, J.F.; Almeida, M.A.; Cunha, M.A. Modelling the ecological patterns of a temperate lagoon in a very wet spring season. *Ecol. Model.* **2010**, *221*, 2302–2322. [CrossRef]

59. Lopes, J.F.; Vaz, N.; Ferreira, J.A.; Dias, J.M. Assessing the state of the lower level of the trophic web of a temperate lagoon, in situations of light or nutrient stress: A modelling study. *Ecol. Model.* **2015**, *313*, 59–76. [CrossRef]

60. Lopes, C.B.; Lillebø, A.I.; Dias, J.M.; Pereira, E.; Vale, C.; Duarte, A.C. Nutrient dynamics and seasonal succession of phytoplankton assemblages in a Southern European Estuary: Ria de Aveiro, Portugal. *Estuar. Coast. Shelf Sci.* **2007**, *71*, 480–490. [CrossRef]

61. Silva, J.F.; Duck, R.W.; Hopkins, T.S.; Rodrigues, M. Evaluation of the nutrient inputs to a coastal lagoon: The case of the Ria de Aveiro, Portugal. *Hydrobiologia* **2002**, *475–476*, 379–385. [CrossRef]

62. ModelRia. *Modelação da Qualidade da Água na Laguna da Ria de Aveiro*; Final Report; Universidade de Aveiro-Centro das Zonas Costeiras e do Mar, Instituto Superior Técnico-Centro de Ambiente e Tecnologias Marítimos and Hidromod: Aveiro, Portugal, 2003.

63. Prescott, J.A. Evaporation from water surface in relation to solar radiation. *Trans. R. Soc. S. Aust.* **1940**, *40*, 11–118.

64. Taylor, K.E. Summarizing multiple aspects of model performance in a single diagram. *J. Geophys. Res.* **2001**, *106*, 7183–7192. [CrossRef]